A BUBBLE CHAMBER STUDY OF PION PHOTO PRODUCTION FROM HYDROGEN

J. M. SCARR.

CONTENTS.

I. Preface.

This thesis describes work carried out by the author in the Department of Natural Philosophy, Glasgow University during the period October 1957 to December 1961.

The introductory chapter reviews the state of knowledge of π^+ - photoproduction from protons and its relation to pion-nucleon scattering up to the later part of 1960 and thus includes data not available at the commencement of this work in 1958. At that time the only extensive data available on π^+ - photoproduction from hydrogen was that of Beneventano et al.(1956). Recent data published on π^+- photoproduction is referred to in the final sections of the thesis.

The second chapter , describes the bubble chamber and its operation with a high energy photon beam. The method of film analysis is also described.

The bubble chamber used in this work, was first tested and brought into operation by the designer, Mr. A. McFarlane, and the present author. The adaption for operation with a target material contained inside a tube passing through the centre of the chamber was the work of the author who was also responsible for the design of the illumination and photographic systems and the electronics controlling chamber operation. Operating behaviour was studied by the author to determine optimum

conditions of temperature and expansion ratio and enabled a useful increase of cycling rate to be obtained.

The details of γ-beam collimation were chosen in the light of experience in collaboration with Dr. I.S. Hughes.

The analysis of photographs was based on a method suggested by the author, measurements being made on an existing projection table. The spatial analysis of the measured events was carried out in collaboration with Dr. W. Morton who wrote the programme used in computation of particle directions and energies.

The third chapter deals with the treatment carriedout by the author of the results obtained after track analysis. The resulting data are discussed and compared with theoretical predictions and recent experimental data given by other workers.

1. The General Features of Photoproduction from Hydrogen.

The possibility of photoproduction of the π-meson or pion from hydrogen was first shown by McMillan, Peterson and White (1949) for the reaction

$$\gamma + p \rightarrow \pi^+ + n \quad . \qquad (1)$$

π^o- production

$$\gamma + p \rightarrow \pi^o + p \qquad (2)$$

was first studied by Panofsky, Steinberger and Stellar (1952). Since these first experiments both reactions have been extensively studied.

The pion is known to be a pseudoscalar particle. The reactions

$$p + p \rightarrow d + \pi^+ \qquad (3)$$

$$\text{and} \quad d + \pi^+ \rightarrow p + p \qquad (4)$$

can be related by detail balancing, a relation which depends on the pion spin. Comparison of Whitehead and Richman's data (1951) on reaction (3) and the π^+ absorption in deuterium data of Durbin, Loar and Steinberger (1951) leads to assigning spin zero to the π^+.

The decay of the π^o - meson

$$\pi^o \rightarrow 2\gamma \qquad (5)$$

indicates (Yang:1950) that the π^o cannot have spin 1.

It is therefore reasonable to assume spin zero for π^+ , π^- and π^o - mesons.

Panofsky, Aamodt and Hadley (1951) studied the absorption of π^- on deuterium. They showed that

$$\pi^- + d \rightarrow 2n \qquad (6)$$

occurs. Since the pion is absorbed from an S-state (Brueckner et al:1951) the π^- parity must be negative. Similarly the absorption of π^- on hydrogen showed the occurence of

$$\pi^- + p \rightarrow n + \pi^o \qquad (7)$$

indicating the equality of π^- and π^o parities, since the reaction would be hindered if π^o emission was not into an S-state because of the low energy release.

Thus the pion is shown to have zero spin and negative parity and the pion is consequently described by a pseudoscalar field.

This conclusion greatly limits the possible pion-nucleon interactions we may consider. The assumption that pions are emitted or absorbed singly, required the interaction to be linear in the pion field variable. Relativistic invariance requirements further restrict the possibilities to two.

where G and F are the coupling constants, ψ the Dirac nucleon spinor, $\underline{\tau}$ the isotopic spin operator, $\underline{\phi}$ the π-field operator. $\vec{\gamma}$, γ_0 and γ_5 are the 4×4 matrices of the Dirac equation. M is the nucleon mass and μ the π-meson mass.

These two possibilities of pion-nucleon interaction with a pseudoscalar pion field are

Pseudoscalar coupling:

$$H_{PS} = -i G \bar{\psi} \gamma_5 \underline{\tau} \cdot \underline{\phi} \psi \qquad (8)$$

Pseudovector coupling:

$$H_{PV} = \frac{F}{\mu} \bar{\psi} \gamma_5 \left\{ \left(\vec{\gamma} \cdot \vec{\nabla} - \gamma_0 \frac{\partial}{\partial t} \right) \underline{\phi} \cdot \underline{\tau} \right\} \psi \qquad (9)$$

For discussion of photoproduction the electromagnetic field which is coupled to the charged pion field must also be included.

In the lowest order perturbation calculations, performed in a power series of coupling constant, the two couplings are equivalent if

$$G = \frac{2M}{\mu} F \qquad (10)$$

Higher order terms occur as divergent integrals. While the P.V. coupling cannot therefore be used in its local form, P.S. coupling yields to mass and charge renormalisation as practised in quantum electrodynamics. Unfortunately the role of γ_5 appearing in the P.S. interaction Hamiltonian is to couple nucleon and anti-nucleon spinors resulting in the production of virtual nucleon - anti-nucleon pairs being very probable.

Further the value of the coupling constant is large. These facts make calculation beyond the insufficient first order approximation very difficult.

These difficulties led to an interpretation of early experiments purely in terms of general conservation laws. Partial wave analyses have been used for both pion-nucleon scattering and photoproduction and since the range of the pion-nucleon interaction is small , $\sim \hbar/\mu c$, we expect that only a few partial waves should suffice.

The considerations of angular momentum and parity give the following possible transitions for photoproduction from nucleons at low angular momenta.

Table I.

γ-transition	Intermediate State	Final State	Angular Distrib.	Momentum dependance of
Ed	1/2 -	$S_{1/2}$	Const	q
	3/2 -	$D_{3/2}$	$2 + 3 \sin^2\theta$	q^5
Md	1/2 +	$P_{1/2}$	Const	q^3
	3/2 +	$P_{3/2}$	$2 + 3 \sin^2\theta$	q^3
Eq	3/2 +	$P_{3/2}$	$1 + \cos^2\theta$	q^3
	5/2 +	$F_{5/2}$	$1 + 6 \cos^2\theta - 5 \cos^4\theta$	q^7

The angular distributions given are for the pure final state. The momentum dependence

$$\sigma_T \propto q^{2l+1}$$

(q = pion centre of mass momentum)

holds at low energies.

Steinberger and Bishop (1952) using a liquid hydrogen target and Janes and Krausbaar (1954) by polythene - carbon subtraction used scintillation telescopes to measure differential cross sections for π^+ production from hydrogen at 90° lab. over the range 165 - 312 mev. Bernardini and Goldwasser (1954 a,b) used nuclear emulsions at several angles round a gaseous target. These measurements were later extended by Beneventano, Bernardini et al.(1956). Other references to experimental work are listed in Appendix I.

These experiments showed the cross section varying proportionally to the meson centre of mass momentum and the low energy angular distribution to be effectively isotropic thus indicating the importance of S-wave π^+ - photoproduction at low energy.

Experiments on π^o- photoproduction from hydrogen by Goldschmitt-Clermont et al.(1953 a) who observed recoil protons in emulsions, Silverman and Stearns (1952) and Mills and Koester (1955) using scintillation telescope to detect a single π^o - decay photon, showed this was not the

case in π^o-photoproduction. The cross-section rises as q^3 indicating the dominance of p-wave production even close to threshold.

The work of Goldschmitt-Clermont et al. (1953 a) and Luckey et al. (1959) shows the angular distribution to be far from isotropic at 170 - 175 mev, the former workers estimating S-wave production at not more than 3%.

As the energy rises above threshold p-wave production plays an increasingly important part in π^+ - photoproduction and the angular distribution is no longer isotropic.

Bruecker (1952) suggested on theoretical grounds that pion-nucleon interactions should involve the existence of a nucleon isobar with T = 3/2 and J = 3/2, which would give rise to resonance effects.

The pion-nucleon scattering experiments of Anderson, Fermi et al. (1953) and Fermi et al.(1953) suggested the existence of a resonance corresponding to a pion centre of mass energy of 150 mev. They found that the ratios of the total cross sections for

$$\begin{aligned} \pi^+ + p &\longrightarrow \pi^+ + p \\ \pi^- + p &\longrightarrow \pi^- + p \\ \pi^- + p &\longrightarrow \pi^o + n \end{aligned} \qquad (11)$$

in the neighbourhood of the resonance were 9: 1: 2. This fact is simply explained by the assumption of charge independence and the dominance of the T = 3/2 interaction. The value of the cross-section at resonance indicates the resonant state to be J = 3/2. Phase shift analysis carried out by many workers shows the (3/2, 3/2) phase shift δ_{33} becomes 90° at about 195 mev confirming the existence of a resonance, (Chiu and Lomond, 1959).

It is reasonable to suppose that this resonance would also appear in pion-photoproduction at the appropriate energy. Consequently Walker, Teasdale et al. (1955) and Tollestrup et al. (1955) measured π^+- angular distributions for incident photons in the energy range $E\gamma$ = 200 - 470 mev using magnetic spectrometer and counter telescope systems respectively. Their results show a maximum total cross section for π^+ photoproduct of $21.10^{-29} cm^2$ at 320 mev. Above this maximum the cross section falls off faster than λ^2 (λ = photon wave length), a behaviour expected above a resonance.

The angular distribution at 320 mev is approximately of the form $2 + 3 \sin^2\theta$. Which agrees with the supposition of a magnetic dipole transition to a J = 3/2

state.

A similar behaviour is shown in π^o photoproduction where Walker, Oakley and Tollestrup (1955) observe the angular distribution at 300 mev to be of the $2 + 3 \sin^2\theta$ form.

Oakley and Walker (1955) and McDonald, Peterson and Corson (1957) have together covered the angular range 30^o - 150^o for π^o - production for photon energies from 260 to 450 mev. They show the cross section reaches a maximum of 27.10^{-29} mev at 320 mev with a rapid fall off of cross section at higher energies. Their results confirm the $2 + 3 \sin^2\theta$ dependence of angular distribution in the region around 300 mev. The fact that the π^o cross section at resonance is greater than that for π^+ production suggests the $T = 3/2$ final state to be the more important.

The forementioned experiments thus lead to the conclusion that the magnetic dipole transition to a $T = 3/2$, $J = 3/2$ state plays a major part in pion-photoproduction from hydrogen and results in the appearance of a resonance for photon energies near 300 mev. At energies close to threshold it is seen that while π^o - production is still mainly p - wave, π^+ production has an important s - wave contribution.

Watson et al.(1956) have made a detailed analysis

along these lines for energies up to resonance. Their analysis shows that besides production by magnetic dipole transition into the T = 3/2 J = 3/2 state other p-wave modes must also be included and possibly some D-waves interference terms as well.

If S and P-wave production is considered together with D-wave interference effects, the differential cross section may be written in the form

$$\frac{d\sigma}{d\Omega} = A + B \cos\theta + C \cos^2\theta \qquad (12)$$

The coefficients A,B and C are related to the transitions shown in Table I by the relations

$$\begin{aligned} A &= |Ed|^2 + \tfrac{1}{2}\left(|U|^2 + |V|^2\right) \\ B &= -2\,\mathrm{Re}\,(Ed^*K) \\ C &= |K|^2 - \tfrac{1}{2}\left(|U|^2 + |V|^2\right) \end{aligned} \qquad (13)$$

where

$$\begin{aligned} U &= 2M_\alpha(3/2) + M_\alpha(1/2) \\ V &= M_\alpha(3/2) - M_\alpha(1/2) + \tfrac{1}{2}\,Eq \\ K &= M_\alpha(3/2) - M_\alpha(1/2) - \tfrac{1}{2}\,Eq \end{aligned} \qquad (13a)$$

Each of the transition amplitudes in (13a) correspond to a final state of given angular momentum.

These amplitudes can be further subdivided into parts leading to final states with T = 1/2 and T = 3/2. The resulting complex amplitudes can be related to the pion-nucleon scattering phase shifts by the requirement of unitarity for the S-matrix covering all scattering and photoproduction channels. The phases of the photoproduction amplitudes are then given by the pion-nucleon phase shifts and the four elementary photoproduction processes can be described by 12 real quantities for energies up to resonance. The expressions for the amplitudes of (13a) have been given by Gell-Mann and Watson (1954).

Beneventano, Bernardini et al. (1956) have used equation (12) to analyse the angular distributions for π^+ photoproduction on hydrogen. However, this form of angular distribution, although suitable for discussion of π^o - production is incomplete when π^+- production is considered.

All the theories (Marshak, 1952) of charged photoproduction give rise to a term in the matrix element

$$\frac{\underline{\sigma} \cdot (\underline{k} - \underline{q})\ \underline{q} \cdot \underline{\varepsilon}}{q_o k - \underline{q} \cdot \underline{k}} \qquad (14)$$

where $\underline{k}, k$ is the photon momentum, energy and $\underline{q}$, q_o the meson momentum, energy in the centre of mass system and $\underline{\varepsilon}$ and $\underline{\sigma}$ are the photon polarisation and nucleon spin respectively.

This term occurs in the lowest order calculations and arises from the direct interaction of the electromagnetic field with the meson field. Since this term contributes to all partial waves charged pion photoproduction cannot be represented completely by (12).

The variations from Eq (12), introduced by inclusion of the direct interaction or retardation term, are most apparent at energies well above threshold and for production at forward angles.

Consequently experiments have been performed by Malmberg and Robinson (1958), Uretsky et al.(1958), Lazarus, Panofsky et al. (1959) and Knapp et al. (1959) for photon energies from 220 to 390 mev with emphasis on π^+ - production at forward angles.

These experiments show that when results at small angles are included, the angular distributions cannot be fitted by (12) but give better agreement with the theory of Chew et al. (1957) which includes the retardation term.

Moravesik (1956) pointed out the importance of the retardation term in analysis of π^+ photoproduction. The addition of the retardation term to the photoproduction matrix element as used by Gell-Mann and Watson (1954) leads to a representation of the angular distribution by

$$(1 - \beta \cos\theta)^2 \frac{d\sigma}{d\Omega} = \sum_{n=0}^{4} A_n \cos^n\theta \qquad (15)$$

where $\beta = q/q_0$ is the meson velocity in the centre of mass. Knapp et al. (1957) showed (15), unlike Eq(12), to be capable of representing the data.

We now have for the angular distribution

$$\frac{d\sigma}{d\Omega} = \frac{2e^2f^2}{\mu^2}\frac{q}{k}\Big\{ |E_d|^2 + \tfrac{1}{2}(|U|^2+|V|^2) + \tfrac{1}{2}|R|^2\beta^2\frac{\left(1-\frac{2q}{k}\cos\theta+\left(\frac{q}{k}\right)^2\right)\sin^2\theta}{(1-\beta\cos\theta)^2}$$
$$- 2\,\mathrm{Re}(E_d^* K)\cos\theta + \left[|K|^2 - \tfrac{1}{2}(|U|^2+|V|^2)\right]\cos^2\theta$$
$$- \mathrm{Re}(E_d^* R)\beta\frac{q}{k}\frac{(1-\cos^2\theta)}{(1-\beta\cos\theta)} + \mathrm{Re}(R^* V)\beta\left(\frac{1-q/k\cos\theta}{1-\beta\cos\theta}\right)(1-\cos^2\theta)$$
$$+ \mathrm{Re}(R^* K)\beta\frac{q}{k}\cos\theta\left(\frac{1-\cos^2\theta}{1-\beta\cos\theta}\right)\Big\}$$

(16)

The coefficients Ed, U, V and K are as defined above for equation (13) except for the factor $\frac{2e^2f^2}{\mu^2}\frac{q}{k}$

shown explicitly here. R is the amplitude of the retardation term.

2. Photoproduction of π^+ near threshold

Apart from the general relationship between pion-nucleon scattering and π^+ - photoproduction derived from S-matrix properties a further relationship exists as indicated by Marshak (1951) and Anderson and Fermi (1952). This relationship holds at threshold and also involves measurements of the Panofsky ratio.

Panofsky et al. (1951) observed the absorption of negative pions by hydrogen at zero energy. Two reactions occured on absorption of the π^-, charge-exchange scattering

$$\pi^- + p \longrightarrow \pi^o + n \qquad (17a)$$

and radiative absorption,

$$\pi^- + p \longrightarrow n + \gamma \qquad (17b)$$

The Panofsky experiment measured the ratio

$$P = \frac{\text{rate } (\pi^- + p \longrightarrow \pi^o + n)}{\text{rate } (\pi^- + p \longrightarrow n + \gamma)}$$

The important point is that Wightman (1950) and Brueckner et al. (1951) have shown that the absorption of the π^-, which takes place after the pion is captured into an orbital round the proton is extremely unlikely from any but the K-shell. In other words

In other words the Panofsky experiment observes a purely S-wave pion-nucleon interaction.

As a result reaction (17b) is directly related to the inverse reaction, photoproduction at threshold

$$\gamma + n \rightarrow \pi^- + p \qquad (18)$$

, which is also purely s-wave, by detailed balance.

Thus we have

$$\sigma(\pi^- + p \rightarrow \pi^0 + n) = P_\chi 2 \left(\frac{K}{q}\right)^2_\chi \sigma(\gamma + n \rightarrow p + \pi^-) \qquad (19)$$

Unfortunately $\sigma(\gamma + n \rightarrow p + \pi^-)$ must be inferred from experiments on deuterium. The ratio

$$R = \frac{\sigma(\gamma + n \rightarrow \pi^- + p)}{\sigma(\gamma + p \rightarrow \pi^+ + n)} \qquad (20)$$

is deduced from measurements of

$$R^1 = \frac{\sigma(\gamma + d \rightarrow \pi^- + 2p)}{\sigma(\gamma + d \rightarrow \pi^+ + 2n)} \qquad (21)$$

The behaviour of $\sigma(\gamma + p \rightarrow \pi^+ + n)$ in the photon energy range 170 - 230 mev has been measured by Beneventano, Bernardini et al. (1956). Their results indicate that

$$a_0^+ = \frac{1}{W} \frac{d\sigma}{d\Omega}(90^\circ \text{ C.M.}) = 14,8 \pm 0,2 \cdot 10^{-30} \text{ cm/ster}$$

over the range of measurement, where $W = 99\%\left(1+\frac{K}{M}\right)^{-2}$
Since the retardation term vanishes at threshold the total cross section at threshold is given by

$$\sigma_T(\gamma \to \pi^+) = 4\pi\, a_0^+(q=0) \times W(q=0)$$

Assuming a_0^+ remains constant down to threshold we obtain close to threshold the total cross section

$$\sigma_T(\gamma \to \pi^+) = 1{,}43 \pm 0{,}02 \cdot 10^{-28} \left(q/\mu\right) \text{ cm}^2. \qquad (22)$$

The ratio (20) must be deduced from measurements of the π^-/π^+ ratio from deuterium.

Sands et al.(1954), Beneventano et al. (1958) and Hogg and Bellamy (1958) have measured the $n_D^-/n_D^+ = R$ ratio by detecting the charged pions produced and show that the ratio rises as lower pion energies are observed.

Since we no longer have a two-body interaction a given pion energy cannot be related to a unique photon energy. It appears reasonable, however, that the impulse approximation (Chew, Goldberger(1952); Chew, Wick, (1952)) is applicable to photoproduction in deuterium since the nucleons are widely separated compared with the pion and photon wavelengths (Lederman, Rogers (1957)) and are weakly bound. The spectrum of photon-energies corresponding to a given pion energy gives a mean photon energy close to that given by two

body kinematics.

The experiments indicate a value of $N_d^-/N_d^+ \simeq 1.6$ for the π^-/π^+ ratio at threshold measured in deuterium. To obtain the threshold value for the ratio from free nucleons, corrections must be made to allow for the final state interactions arising from the presence of an extra nucleon. Charge symmetry indicates identical nuclear interactions for

$$\begin{aligned} \gamma + d &\rightarrow \pi^- + p + p \qquad (a) \\ \gamma + d &\rightarrow \pi^+ + n + n \qquad (b) \end{aligned} \tag{23}$$

and consequently coulomb effects alone, present only in π^- production, need be considered in reducing the ratio N_D^-/N_D^+ measured in deuterium to the π^-/π^+ ratio for free nucleons.

The most complete calculation has been given by Baldin (1958) who calculated the effect of both nuclear and coulomb interactions. The coulomb effects are due to interaction between all 3 final state particles in reaction (23a) and causes $\sigma(\gamma + d \rightarrow \pi^- + 2p)$ to rise up steeply above $\sigma(\gamma + n \rightarrow \pi^- + p)$ at photon energies below 170 mev. Nuclear interactions between the final states have a smaller but opposite effect reaching to higher energies.

Application of the Baldin corrections to the data of Sands et al. (1954), Beneventano et al. (1958) and Hogg and Bellamy (1958) suggests a threshold value of R = 1,3. Hence the threshold value for π^- production from neutrons is

$$\sigma_T (\gamma \rightarrow \pi^-) = 1.86 \ .10^{-28} (\frac{q}{\mu}) \ cm^2. \qquad (24)$$

using the value of Eq(22).

The experimental values mentioned above depend upon the validity of the impulse approximation and upon the assumption that the use of two body kinematics is a sufficiently good approximation.

Adamovich et al. (1959) have studied the reaction

$$\gamma + d \longrightarrow \pi^- + p + p$$

using emulsions loaded with deuterium. The method has the advantage that all final particles are detected and hence the photon energy can be unambiguously determined. Their experiment also gives support to the validity of the impulse approximation when final state interactions are considered. By selection of final particle momenta, so as to obtain maximum validity of the impulse approximation and to minimise the coulomb interaction between pion and protons Adamovich et al.

found a_o^- to be constant in the range 157 - 180 mev

$$a_o^- = 19.1 \pm 2,1. \ 10^{-28} \ cm^2/ster.$$

Although this value is consistent with the value of a_o^+ measured by Beneventano et al.(1956) for R = 1,3 Adamovich et al. (1960) obtained a value for a_o^+ appreciably higher than Beneventano et al. The Adamovich value is consistent with a_o^+ constant in the range 153 - 175 mev with a value

$$a_o^+ = 18. \ 10^{-30} \ cm^2/ster.$$

Adamovich et al. (1960) give an improved and corrected value for a_o^- which combined with their value for a_o^+ gives a value R = 1.3 $\pm$ 0.15.

It should be pointed out that there is no theoretical justification for a_o^+ and a_o^- being constant up to threshold. However, if the extrapolations of π^+ and π^- results are handled similarly the exact method of extrapolation used has little effect on the π^-/π^+ ratio from free nucleons , though naturally affecting the absolute values of the threshold cross sections.

The discrepancy between the threshold values obtained by Adamovich et al. and Beneventano et al. may be due to the values of a_o^+ and a_o^- not being constant down to threshold. However the two experiments do not

give very good agreement for a_o^+ where the measurements are performed at similar energies. The difference could lie in differences of beam monitoring for the two experiments.

The value for the cross section for

$$\gamma + n \rightarrow \pi^- + p$$

at threshold obtained from photoproduction experiments is to be compared with the value deduced from charge-exchange scattering at zero energy.

Charge-exchange scattering of pions on protons

$$\pi^- + p \rightarrow \pi^o + n$$

has been measured by Spry (1954) and Tinlot and Roberts (1954) for pion energies in the range 20 - 40 mev , and Bodansky et al. (1954) at 65 mev. Kernan et al.(1960) give measurements at 61 and 95 mev. However, because of the scarcity of information particularly at low energies where the experiment becomes difficult, it is usual to include data from both π^+ and π^- elastic scattering in determining the zero energy cross section for charge exchange scattering.

This proceedure depends on the aplicability of charge independance to pion-nucleon scattering. The validity

of this assumption was first shown by Anderson, Fermi et al. (1952 a,b) and is confirmed by the success of the phase shift analysis of pion-nucleon scattering.

Since at low energy the scattering process is entirely S-wave, the charge exchange total cross section is given by

$$\sigma_T(\pi^- \rightarrow \pi^0) = \frac{8\pi}{9}\lambda^2(\delta_1 - \delta_3)^2 \frac{v_0}{v_-} \qquad (25)$$

where δ_1 , δ_3 are the s-wave phase shifts for the $T = 1/2$ and $T = 3/2$ states respectively. (v_0/v_-) the ratio of centre of mass meson velocities allows for the π^-, π^0 mass difference. (Schiff:1955).

Orear (1956) has analysed pion-nucleon scattering data up to 65 mev and concludes

$$(\delta_1 - \delta_3) = (0{,}272 \pm {,}016)\ q/\mu$$

Combining the Orear values with the threshold π^0 velocity $V_0 = 0{,}20 \pm 0{,}01$ C given by Chinowsky and Steinberger (1954) we have the threshold value

$$\sigma_T(\pi^- \rightarrow \pi^0) = 8{,}25 \cdot 10^{-28}(\mu/q) \quad cm^2.$$

where q is the π^- meson momentum.

Using the Panofsky ratio and detailed balance we

can arrive at a value for $\sigma(\gamma \rightarrow \pi^-)$ which can be compared with the value obtained from photoproduction experiments.

The ratio

$$P = \frac{\text{rate } (\pi^- + p \rightarrow \pi^o + n)}{\text{rate } (\pi^- + p \rightarrow \gamma + n)}$$

measured at zero energy was first measured by Panofsky et al.(1951) as 0,94. The importance of the ratio lies in the entirely S-wave nature of the reactions.

Table III shows the experimental values obtained for the Panofsky ratio.

Table II

Panofsky et al.(1951)	0,94 ± 0,30	Pair Spectrometer
Lederman et al.(1956)	1,10 ± 0,50	
Cassels et al. (1957)	1,50 ± 0,15	Cerenkov counter
Fischer et al. (1958)	1,87 ± 0,10	"
Knenher et al. (1959)	1,60 ± 0,17	Pair Spectrometer
Koller and Sachs(1959)	1,46 ± 0,10	Cerenkov counter
Derrick (1960)	1,51 ± 0,10	Bubble Chamber
Dunaitsev et al.(1960)	1,40 ± 0,08	γ-γ coincidences
Samois (1960)	1.62 ± 0.06	Bubble Chamber
Jones (1961)	1,56 ± 0,05	Cerenkov counter.

The earlier data seem to show inconsistencies. The charge exchange produces a π^o of velocity 0,20C which on decay into two photons gives rise to a flat γ-spectrum ranging from 55 - 83 mev. The radiative absorption produces a line spectrum at 129 mev. Both Pair spectrometer and Cerenkov counters have been used to determine the relative intensities of these two spectra.

The Cerenkov experiments unfortunately are not able to resolve completely the two spectra. Particularly in the earlier experiments this limited the accuracy of the result. The individual spectrum shapes are determined by observing γ-γ coincidences for the π^o-decay spectrum and delayed neutron γ-coincidences for the 129 mev line. Reduced counting rate and uncertainty of counting efficiency prevented the Panofsky ratio being determined from the separate spectra. Systematic errors in these spectra due to unsuspected variation of efficiency with energy would considerably affect the result obtained.

Fischer et al.(1958) and Köller and Sachs(1959) convert the γ-rays in the Cerenkov counter. Since the shower electrons are highly relativistic, if they are contained, the intensity of Cerenkov light is very nearly proportional to the photon energy. Systematic errors may arise from scattering in the defining aperture.

Cassels et al. (1957) and Jones et al. (1961) use a lead converter defining the aperture with a scintillator. This reduces the efficiency and makes it energy dependant.

The experiments of Panofsky et al. (1951) and Kuenher et al. (1959) used pair spectrometers for photon detection and were able to separate the two spectra. Kuenher et al. used a 180^{o} pair spectrometer and fitted the spectra with calculated resolution curves. The major correction in these experiments is for the energy dependance of pair production. Kuenher et al. have a correction of only 1% for the overlap of spectra.

Samois (1960) and Derrick et al.(1960) use liquid hydrogen bubble chambers to detect internally converted pairs from the two reactions. These independant results are in agreement with the other methods.

It seems fairly certain we can rely on a value for the Panofsky ratio of

$$P = 1,53 \pm ,03$$

a value deduced from the more recent results. Combining the values

$$P = 1,53 \pm ,03$$

$$\sigma_T(\pi^- \rightarrow \pi^o) = 8,25. \ 10^{-28} \left(\frac{\mu}{q}\right)_{E=o} \ cm^2$$

in equation (19)

$$\sigma_T(\gamma + n \rightarrow p + \pi^-) = \frac{1}{2P}\left(\frac{q}{k}\right)^2_{q=o} \times \sigma_T(\pi^- \rightarrow \pi^o)$$

one obtains

$$\sigma(\gamma + n \rightarrow p + \pi^-) = (3{,}00 \pm 0{,}24).10^{-28}(q/\mu)\ cm^2$$

This value is too large compared with the results deduced from photoproduction

Bernardini	$(1{,}86 \pm {,}19).10^{-28}\ (q/\mu)\ cm^2$
Adamovich	$(2{,}19 \pm 0{,}23)\ 10^{-28}(q/\mu)\ cm^2$

to be attributable to statistical errors. The "Bernardini" result depends on π^-/π^+ ratio results of other workers besides those of Beneventano et al. The difference between Adamovich and Bernardini results (15%) probably arises partly from the difficulty of bremsstrahling beam calibration. The value for $\sigma(\gamma \rightarrow \pi^-)$ deduced from scattering data appears beyond the uncertainty of beam calibration which is probably around 10%. We shall return to this discrepancy in a later section.

3. Recent Theory of the Pion-Nucleon Interaction.

The previous section shows up some inconsistencies in the relation between low energy pion-nucleon scattering and pion-photoproduction data. In order to discuss this problem it is useful to make use of some theoretical guidance which can be obtained from recent theoretical work.

We have seen in a previous section that the possible relativistically invariant pion-nucleon interactions do not yield to more than an insufficient first order approximation.

One of the difficulties of using the pion-nucleon interaction

$$-iG\,\bar{\psi}\,\gamma_5(\underline{\tau}\cdot\underline{\phi})\,\psi \qquad (26)$$

is the importance of nucleon anti-nucleon pairs. These nucleon anti-nucleon pairs are eliminated if we consider the non-relativistic limit for the nucleons when (26) reduces to

$$i\frac{\mu G}{2M}\,\phi^{*}\,\vec{\sigma}\cdot\vec{q}\,(\underline{\tau}\cdot\underline{\phi})\,\phi \qquad (27)$$

where ϕ is a Pauli spinor.

Since we have introduced an extra power of meson

momentum in (27) the interaction leads to divergences unless we replace the point interaction by a non-local interaction, the nucleon being spread out.

This spreading out of the region of interaction is equivalent to the introduction of a cut-off momentum q_{max}. For a source density $\rho(\underline{r})$ the interaction becomes

$$H_{int} = \int F \rho(\underline{r}) \vec{\sigma} \cdot \vec{\nabla} (\underline{\tau} \cdot \underline{\phi}) \vec{dr} \qquad (28)$$

This "static" or "cut-off" theory is therefore described by two parameters, the cut-off energy and the coupling constant

$$F = \frac{\mu G}{2M} \qquad (29)$$

and is limited to energies at which both initial and final nucleon are non-relativistic.

Chew and Low (1956) have presented the theory for pion-nucleon scattering and for photomeson production. The interaction for photoproduction is obtained by the substitution

$$\vec{\nabla} \phi \longrightarrow (\vec{\nabla} - ie \vec{A}) \phi \qquad (30)$$

in the interaction Lagrangian Lint = - Hint. The retardation term is obtained using this substitution on the free field Lagrangian.

Though this substitution is correct for a local interaction it does not lead to exact gauge invariance with an extended source. The necessary extra terms are not well defined but fortunately they appear unimportant for photoproduction at energies for which the static approximation is applicable.

The theory has been summarised for pion-nucleon scattering by Wick (1955) and Chew (Handbuch der Physik, 43). Chew also discusses photoproduction.

The"cut-off" theory gives a better representation of scattering and photoproduction than previous theories.

The theory is limited in that the interaction (28) gives only a P-wave interaction between pion and nucleon. Nucleon recoil effects are also neglected.

Chew showed that the first order calculation is insufficient and that higher orders are necessary.

More recently dispersion theory has been applied to pion-nucleon interactions as well as other problems. Karplus and Ruderman (1955) showed the practical use of dispersion-relations in meson theory. Goldberger et al.(1955) gave dispersion relations for pion-nucleon

scattering at 0^{o} which were shown by Anderson, Davidson and Kruse (1955) to be in agreement with the experimental results for total scattering cross sections.

Dispersion relations have been extended to other angles by many workers. Chew, Low, Goldberger and Nambu (1957) have applied dispersion theory to pion-nucleon scattering and pion photoproduction. They show that this theory essentially gives the results of the "cut-off" theory. It has however the advantages of being relativistic and including recoil effects and for this reason supercedes the "cut-off" theory.

The dispersion relations indicate the restrictions placed upon the S-matrix required by causality, that is, the requirement that signals cannot propagate with velocity greater than C.

More exactly two assumptions are necessary. Firstly, the assumption of microscopic causality which indicates non-interference of observables at points with space like separation however small the separation. This assumption seems to be strictly applicable only to local field theory. The second assumption postulates that all physical states form a complete set. It is not clear that this is necessarily the case in a local field theory.

However assuming these conditions dispersion relations have been derived in special cases. In many cases dispersion relations, based on perturbation theory, have been assumed.

Goldberger, Miyazawa and Oehme (1955) give forward scattering dispersion relations for pion-nucleon elastic scattering. For charged pions these may be written

$$\frac{1}{2}\left[D_-(k) - D_+(k) \right] = -2f^2 \frac{(\mu^2/2M)^2 - \mu^2}{\omega^2 - (\mu^2/2M)^2} \cdot \frac{\omega}{\mu^2}$$

$$+ \frac{\omega}{4\pi^2} \int_0^\infty k'^2 \frac{\sigma_-(k') - \sigma_+(k')}{\omega'(k'^2 - k^2)} dk' \qquad (31)$$

where D- and D+ are the dispersive (real) parts of the forward scattering amplitude D + i A in the laboratory.

and

$$D_E(k) - D_E(0) = 2f^2 \frac{k^2}{\omega^2 - (\mu^2/2M)^2} \cdot \frac{1}{2M}$$

$$+ \frac{k^2}{4\pi^2} \int_0^\infty \frac{(\sigma_-(k') + \sigma_+(k'))dk'}{k'^2 - k^2} \qquad (32)$$

where $D_E(k) = \frac{1}{2}\left[D_+(k) + D_-(k) \right]$

and $w^2 = k^2 + \mu^2$ is the meson lab energy. A

subtraction is necessary in (32) to obtain convergence.

Puppi and Stanghellini (1957) compared D+ and D- with experiment and found a discrepancy for π^- scattering. Spearman (1960) using the S-wave scattering lengths given by Orear(1956), $a_1 = 0{,}165$ and $a_3 = -0{,}105$, together with $f^2 = 0{,}08 \pm {,}01$ and using better cross section values eliminated this discrepancy. The recent values given by Hamilton and Woolcock (1960)

$$a_1 = 0{,}175 \qquad a_3 = -\,0{,}087$$

improve the fit further. It appears the original discrepancy is resolved using improved data.

Chew, Low, Goldberger and Nambu (1957) give dispersion relations for pion-nucleon scattering at finite angles, and assume the dispersion integrals are dominated by the (3,3) resonance. The results are given to order v/c and thus include some corrections to the static approximation.

They give results for the S , P and D-wave phase shifts. Since only the (3,3) contribution to the dispersion integrals has been used it is unlikely that the small P-wave phase shifts are very reliable. Their results indicate

$$\frac{\delta_1 - \delta_3}{q q_0} = \frac{1}{1 + q_0/M} f_1(q_0^2)$$

$$\frac{\delta_1 + 2\delta_3}{q} = \frac{1}{1 + q_0/M} f_2(q_0^2) \qquad (33)$$

Equations (33) result as a direct consequence of crossing symmetry. In particular Chew et al. give,

$$a_1 - a_3 = q_0 \left\{ 6 f^2 - \frac{4}{\pi} \int \frac{dq'}{q'^2} \frac{\sin^2 \delta_{33}}{q_0'} + \frac{2}{\pi} \int \frac{dq'}{q_0'} \frac{\sin^2 \delta_1 - \sin^2 \delta_3}{(q_0'^2 - q_0^2)} \right\} \qquad (34)$$

which, perhaps fortuitously, agrees reasonably with experimental data. However inclusion of high energy cross sections into the integral would probably require the introduction of a subtraction.

Chew et al. also give dispersion relations for pion photoproduction at nucleons, again assuming the (3,3) resonance dominates the integrals. Their treatment leads to expressions for the amplitudes appearing in Eq(16) for π^+ photoproduction. The resulting expressions are collected into a convenient reference by Lazarus et al.(1959).

The evaluation of the dispersion equations as carried out by Chew et al. (1957) depends on the following assumptions. The dispersion integrals are assumed to

be dominated by the (3,3) resonance to the extent that other contributions can be ignored. In general the integrals contain a contribution arising from non-physical values of the energy variable which has been assumed negligible. Only in the case of momentum transfer equal to the momentum transfer at threshold does this non-physical contribution vanish. This occurs for pion-production at an angle θ' given by

$$k(q_0 - q\cos\theta') = 0.93 \qquad (35)$$

Baldin (1960) points out the better fit of the Chew et al. calculations under this condition.

Mandelstam (1958) has proposed a powerful method in which both energy and momentum-transfer variables are extended into complex variables simultaneously. The Mandelstam representation, together with the unitarity requirements on the S-matrix, appears to be capable of giving a complete theory of strong interactions.

Ball (1960) has used the Mandelstam representation to calculate the effects of a two-pion resonance on photoproduction. The pion-pion coupling constant λ is expected to be of order e. Ball finds a small value of λ having an appreciable effect both on the

threshold photoproduction cross sections and the π^-/π^+ - ratio, for nucleons.

4. The Threshold Problem.

We have seen in a previous section that the value of the zero energy charge-exchange cross section for pion scattering, deduced from results of phase shift analysis using Orear's (1956) values for the scattering lengths a_1 and a_3, does not agree with the value deduced from Bernardini's data on π^+- production.

A solution to this problem was proposed by Cini et al. (1958) who pointed out that the extrapolation of the π^+ photoproduction data of Beneventano et al., by assuming a_o^+ to be constant down to threshold, is not in agreement with the dispersion relations of Chew et al. (1957).

Eq(16) gives the cross section for π^+ photoproduction where the theory of Chew et al.(1957) leads to values for the amplitudes Ed, U, V, K and R. To first approximation (given also by earlier theory)

$$Ed = R = 1$$

when

$$\frac{d\sigma}{d\Omega} = \frac{2e^2 f^2}{\mu^2}\,\frac{q}{k}\left\{1 - \frac{\mu^2}{2k^2}\,\frac{\beta^2 \sin^2\theta}{(1-\beta\cos\theta)^2} + P\text{-wave terms}\right\} \qquad (36)$$

The second term in (36) contains both the pure retardation term and the interference between the S-wave

and retardation term given in Eq(16). The presence of this term predicts a decrease in the value of $|T^+|^2 = \frac{1}{W} d\sigma/d\Omega$ as the energy rises above threshold. Using the behaviour predicted by dispersion theory as a guide for the extrapolation of the experimental data to threshold, a higher threshold value for a_o^+ is obtained

$$a_o^+ = 20.\ 10^{-30}(\frac{q}{\mu})\ \text{cm}^2/\text{ster}$$

Cini et al. (1958) used this value, obtained by normalising the curve given by dispersion theory to the data at 170 mev, to obtain the threshold total cross section

$$\sigma_T(8 \rightarrow \pi^+) = 1.93 \times 10^{-28}(\frac{q}{\mu})\ \text{cm}^2.$$

On the basis of Eq(34) Cini et al. obtain the value

$$a_1 - a_3 = 0,24$$

at zero energy. They used the form

$$(a_1 - a_3) = (Aq_o + Bq_o^3)(1 + {}^{q}\!/_{M})^{-1} \qquad (37)$$

where A = 0,31 and B = 0,0318. The constants were determined by setting $a_1 - a_3 = 0,27$ at both 30 and 150 mev.

A value of $a_1 - a_3$ at zero energy can be also obtained from the forward scattering dispersion relations of Goldberger et al. (1955) from Equation (31). The dispersion integrals are evaluated assuming

$\sigma_-(k') = \sigma_+(k')$ for energies above 2 Bev.

Pomeranchuk (1958) has shown that if $\sigma_-(k)$ and $\sigma_+(k)$ approach constant values at high energies then $\sigma_-(k) = \sigma_+(k)$ at these energies. This is supported by data of Cool et al.(1956) and Lougo et al.(1959). The value $a_1 - a_3 = 0,24$ requires $f^2 \sim 0,075$.

The use of the Cini values with the previous values of Panofsky ratio and π^-/π^+ ratio gives a better agreement than the original values.

We obtain for $\sigma_T(\gamma + n \rightarrow \pi^- + p)$ the values near threshold

	Deduced from photoproduction	Deduced from Scattering
Original Values	$1,86\ (\frac{q}{\mu}).10^{-28} cm^2$.	$3,00\ (\frac{q}{\mu}).10^{-28}\ cm^2$.
"Cini" Values.	$2,50(\frac{q}{\mu}).\ 10^{-28} cm^2$.	$2,34\ (\frac{q}{\mu}).10^{-28} cm^2$.

The treatment of the charge exchange scattering cross-section assumes the validity of charge independence. Even when coulomb effects have been allowed for and purely nuclear phase shifts are used, the $\pi^- - \pi^o$ mass difference should lead to a divergence from charge independance at low energy, because of the momentum difference between the initial and final states. Furthermore at energies below 40 mev the π^- may undergo radiative capture with a probability comparable with that for charge exchange scattering (Angell, Perry (1953)) producing modifications in the phase shifts. Noyes (1956) has estimated these effects as introducing a correction of not more than 10%.

The threshold values obtained by Cini et al.(1958) although improving the consistency of the low energy pion data cannot be taken as final.

The extrapolation of $(\delta_1 - \delta_3)/q$ to $q = o$ as carried out by Cini et al. is rather arbitary and the form of the extrapolation does not represent the available data well.

More recently further experiments on pion-nucleon scattering have attempted to determine the energy dependance of the S-wave phase shifts. Fischer and Jenkins (1959) found

$\delta_{3/q} = -(0,104 \pm ,006)$ in agreement with the Orear (1956) value. However, an equally good fit is given by

$$\delta_{3/q} = -\,0,089\ w \quad \simeq \quad -\,0,089 - 0,045q^2$$

where w + M is the total centre of mass energy. The second value has a non-linear dependence on q as suggested by dispersion theory. Barnes et al.(1960) have analysed π^- and π^+ scattering below 150 mev and obtained

$$\delta_{3/q} = -\,(0,1145 \pm ,0026)$$

$$\delta_{1/q} = 0,205 - 0,09q^2 + 0,018q^4$$

which gives

$$a_1 - a_3 = 0,32$$

a value much higher than that given by Orear and which is incompatible with photoproduction data. A further analysis by Hamilton and Woolcock (1960) gives

$$\delta_{3/q} = 0,087 - 0,07\ q^2$$

$$\delta_{1/q} = 0,178 - 0,01q^2$$

the dependence for δ_3 agreeing well with that previously given by Fischer and Jenkins (1959) . These values give

$$a_1 - a_3 = 0{,}265 \pm {,}007$$

The phase shifts δ_1 and δ_3 are the "nuclear" phase shifts obtained after correction for coulomb effects by the method of Van Hove (1952) plus additional corrections given by Solmitz (1954) . These corrections assume coulomb effects can be ignored within a sphere of radius $r_o \simeq \hbar/\mu c$. Hamilton and Woolcock (1960) show the inclusion of coulomb interference effects for $r < r_o$ reduce the value of $a_1 - a_3$ by 0,02 giving

$$a_1 - a_3 = 0{,}245 \pm {,}007$$

as the value to be used to calculate the zero energy charge-exchange cross section.

The threshold value for π^+- photoproduction given by Cini et al.(1958) is based upon dispersion theory, the theoretical curve being normalised to the 170 mev measurement of Beneventano et al.(1956). It is apparent however, that the experimental data does not agree with the dispersion predictions of Chew et al. (1957) thus limiting the validity of the value of at threshold deduced by Cini et al.

Figure 1 shows a plot of a_o^+, where the solid lines represent the predictions of Chew et al. The quantity $N^{(-)}$ has a small but unknown value which does not affect the shape of the curves.

As a result of this discrepancy between experiment and theory, a number of recent experiments, directed at the measurement of $d\sigma/d\Omega(\gamma + p \rightarrow \pi^+ + n)$ close to threshold, have been performed.

Lewis and Azuma (1959) using a counter telescope system obtained results in agreement with Beneventano et al. Barbaro and Goldwasser (1959) measured the differential cross section at 90^o c.m. at 160 and 219 mev. These results indicated a cross section somewhat higher than those of Beneventano et al. near threshold, but this conclusion rests upon the evidence of a single point.

Gorzhevskaya et al.(1960) and Adamovich et al.(1960) at Lebedev have measured a_o^+ in the range $E\gamma$ = 153 — 175 mev (lab). Although their results indicate a higher value of a_o^+ than indicated by Beneventano et al., they are consistant with a_o^+ constant if considered alone.

The results of Leiss and Penner (1955) for energies close to threshold which originally supported the

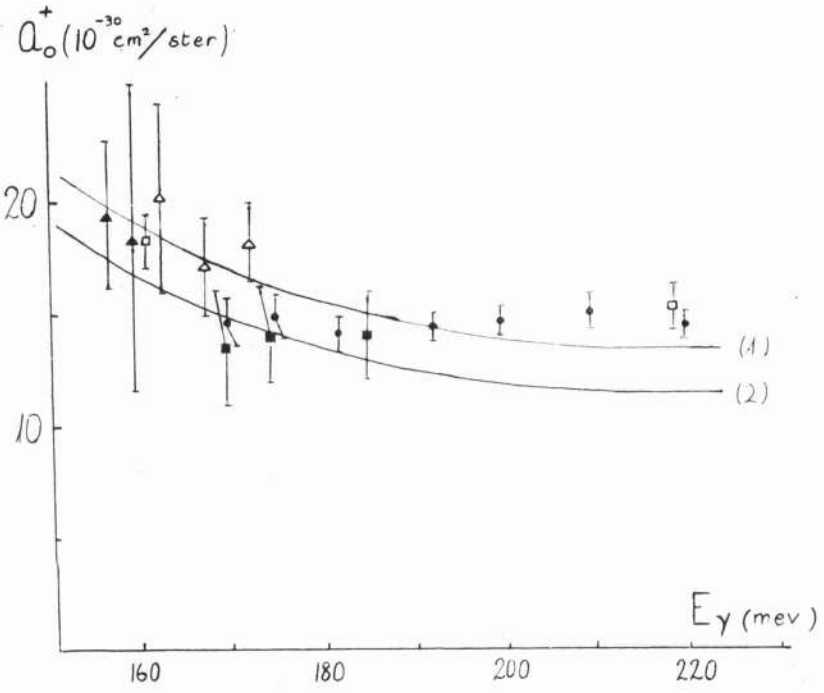

Fig.1. The experimental points for $a_o^+ = \frac{1}{W}\frac{d\sigma}{d\Omega}(90°c.m.)$ given by Gorzhevskaya (1960) ▲, Adamovich et al. (1960) △, Barbaro and Goldwasser (1959) □, Lewis and Azuma (1959) ■, and Beneventano et al. (1956) ●, are compared with the curves given by Dispersion theory. (1) corresponds to $f^2 = 0,08$ and $N^{(-)} = 0$ and (2) to $f^2 = 0,08$ and $N^{(-)} = -0,05$.

constancy of a_o^+ were liable to rather large errors and were in error (Leiss, Penner;(1959)).

All the forementioned results are shown in figure 1. Although the value of a_o^+ tends to rise near threshold this is mainly due to the generally higher values of the lower energy data of Adamovich et al.(1960) and Gorzhevskaya et al.(1960) compared with those of Beneventano et al.(1956). In the energy interval where these two sets of data overlap they do not appear altogether consistent. At 170 mev the Adamovich results are higher by 20%. This difference could arise partly from the difficulties of absolute calibration of a photon beam monitor. Because of the difficulties of beam calibration, the relative errors of a single experiment may be appreciably smaller than the absolute error. For this reason it is advantageous to determine the behaviour of a_o^+ from a single experiment. None of the above experiments, apart from the single low energy point of Barbaro and Goldwasser (1959), considered alone, indicates a tendancy for a_o^+ to increase near threshold. It appears therefore that further experiments covering a wide range of energies are necessary to resolve the problem.

It is also worth noting that the dispersion theory predictions run into difficulties for energies $E^\gamma > 180$ mev where theory predicts values some 20% too low.

To sum up, the threshold cross section

$$\sigma_T(\gamma + p \rightarrow \pi^+ + n) = (1{,}43 \pm {,}02) \cdot 10^{-28}(\frac{q}{\mu}) \text{ cm}^2$$

deduced by Beneventano et al.(1956) is seen to give a serious discrepancy when compared, using a relation suggested by Marshak(1951) and Anderson and Fermi(1952), with the S-wave scattering lengths $a_1 = 0{,}165$ and $a_3 = -0{,}105$ obtained by Orear(1957) for pion-nucleon scattering.

These results were obtained from the experimental data using extrapolations to zero pion momentum which have no strong theoretical justification, particularly in the case of the photoproduction data.

Theoretical guidance can be obtained from dispersion theory which gives the best available description of pion phenomena. In particular, Chew et al.(1957) have given dispersion theory predictions for pion-nucleon scattering and photoproduction. Cini et al.(1958) used these predictions as a basis for a fresh treatment of the data to give

$$\sigma_T(\gamma \rightarrow \pi^+) = 1{,}93 \cdot 10^{-28}(\frac{q}{\mu}) \text{ cm}^2.$$

and

$$a_1 - a_3 = 0{,}24.$$

The use of these values eliminates the discrepancy.

However, the theoretical behaviour of a_o^+

as given by dispersion theory, does not agree with the values deduced from the photoproduction experiments of Beneventano et al.(1956) and Lewis and Azuma(1959) . Further work of Barbaro et al.(1959) and Adamovich et al.(1960) possibly suggests the rise of a_o^+ near the photoproduction threshold, but the evidence of these experiments is not conclusive.

The analysis of recent data on pion-nucleon scattering supports a non-linear behaviour of $\delta_1 - \delta_3$ with respect to q, and leads to lower values of $a_1 - a_3$ than deduced by Orear (1956).

There is, therefore, room for further experimental work both to show unambiguously the behaviour of for photon energies from threshold up to 230 mev and to determine the energy dependence of the S-wave phase shifts, particularly δ_1 for which less data is available.

III. The Bubble Chamber Study of $\gamma + p \rightarrow \pi^+ + n$.

1. The Aim of the Present Work.

At the commencement of the present work, the only data covering a wide range of energies for π^+ photoproduction on hydrogen and reaching down to low energies was that of Beneventano, Bernardini et al. (1956) for photon energies of 170 mev to 230 mev. These results are not consistent with the predictions of dispersion theory as treated by Chew, Low, Goldberger and Nambu (1957).

Later results of Azuma and Lewis (1959) are in good agreement with those of Beneventano et al. (1956). Adamovich et al. (1960) and Gorzhevskaya et al. (1960) obtain results for the energy range 153 - 175 mev. Their results, however, cannot, as indicated in the previous chapter give a convincing answer to the behaviour of the cross section near threshold because of the relatively large statistical errors and possible intercalibration uncertainties between the different experiments.

It is therefore apparent that further experiments are necessary. Since the relative errors in a given experiment are likely to be less than the absolute errors, it is desirable to perform an experiment over a wide range of energies to give a comparison with theory independent of the intercalibration between different experiments which

is necessary at present.

The study of positive pion photoproduction from hydrogen is carried out by observing the production energy and direction of the resulting pions. This information determines completely the kinematics of the reaction

$$\gamma + p \rightarrow \pi^{+} + n.$$

The present experiment uses a propane bubble chamber, in which a high pressure hydrogen gas target is situated, for the detection of the π^{+}. Protons from π^{o}-production are also detected.

This method has the advantage that pions from all production angles between 10^{o} and 170^{o} and corresponding to all photon energies between 165 mev and 211,5 mev are observed simultaneously. This avoids the possibility of systematic errors which might be energy or angle dependant provided a good scanning efficiency is obtained.

The method gives good angular resolution and the particle energies are determined by range - energy relations. The pion tracks can be followed back almost to the target thus giving confirmation of the position of their origin.

The only important correction that is required allows for the geometric efficiency of the chamber and is a purely geometrical calculation.

2. The Propane Bubble Chamber.

The chamber, designed for use with propane is of 5 litres capacity, and is in the form of a short cylinder 25 cms. diameter and 10 cms. deep. The ends are closed by toughened glass windows approximately 45 cms. thick. A short pipe connects the chamber to the piston responsible for chamber expansion. The piston is controlled by compressed air supplied from a compressor. The chamber is maintained at its operating temperature of 55 - 60°C by a surrounding thermostatically controlled water bath.

An experiment in which low energy particles are to be detected must be arranged so that the production of the particles takes place inside the chamber. The permissible size of entry window to a chamber would severely limit the yield from a reaction outside the chamber. Usually, therefore, the chamber liquid is used as target for the incident particles. In the case of photon induced reactions produced by bremsstrahlung, however, it is necessary to have a pure target, since for example with a propane target events in carbon and hydrogen cannot be completely distinguished, since short recoils cannot be observed.

For the present experiment an Aluminium alloy tube 3,81 cms. diameter, has been placed through the centre of the chamber along the horizontal diameter, as shown in

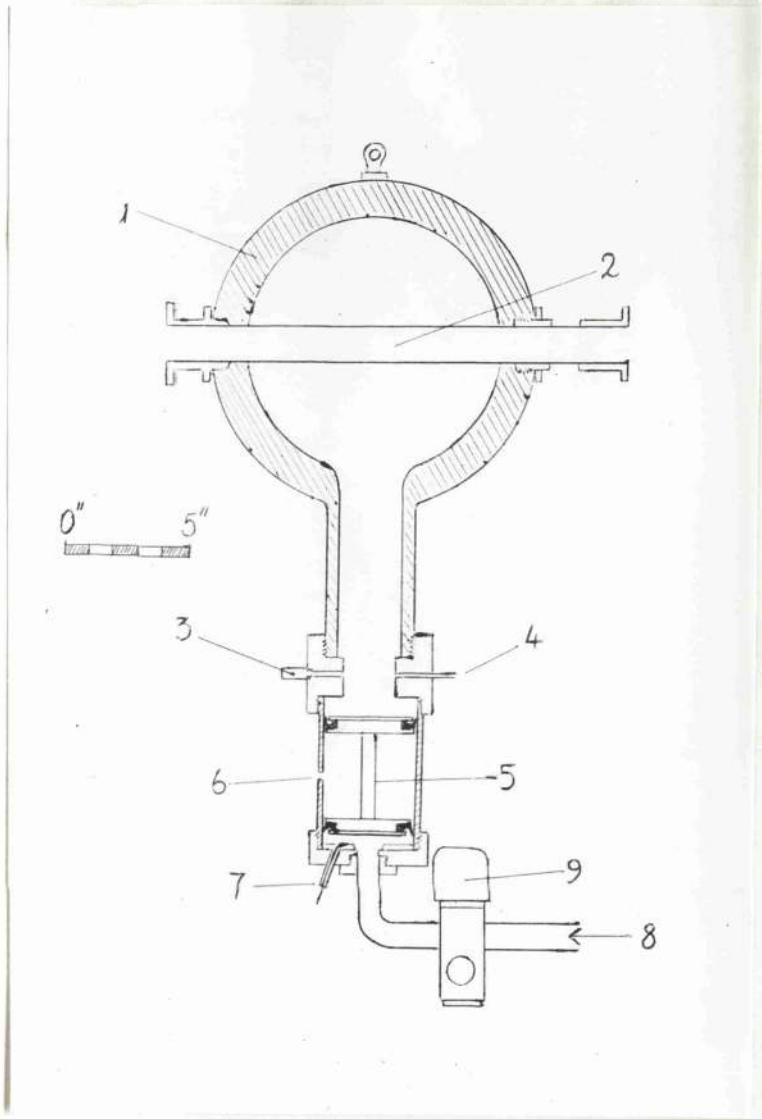

Fig 2. Diagram of the Propane Bubble Chamber. 1. Chamber body. 2. Target-containing tube. 3. Pressure transducer head. 4. Ports for filling chamber, also pressure gauge position. 5. Piston. 6. Aperture in piston wall to maintain atmospheric pressure between piston seals. 7. Electrical contacts (one only shown) which indicate the moment at which expansion is complete. 8. Compressed air input. 9. Barksdale valve.

fig. 2. This target tube, through which the photon beam passes, allows any target material to be contained inside the chamber. Unlike chambers in which the operating liquid is used as the target, the present method allows the target material to be changed without affecting the operation of the chamber. The chamber can also be operated with Freon (CF_3Br) as an operating fluid instead of propane. The increase of density of operating liquid from 0,44 gm. cm^{-2} to 1,5 gm. cm^{-2} allows a higher energy range of reaction products to be stopped in the chamber.

The target tube has a wall thickness of 0,122 cms., sufficient to contain a gaseous target at 42 atmospheres. The minimum detectable particle energy depends only slightly on the thickness of the walls of the target tube. For a two centimetre track in propane corresponding to a pion energy of 13,8 mev the energy loss in the target tube wall is only 2,0 mev or 12½% of 15,6 mev, the minimum detection energy for pions produced at 90^{o} in the laboratory coordinates. The minimum particle energy that can be detected thus depends primarily on the operating liquid in the chamber.

The piston responsible for the expansion of the chamber is operated by compressed air the flow of which is

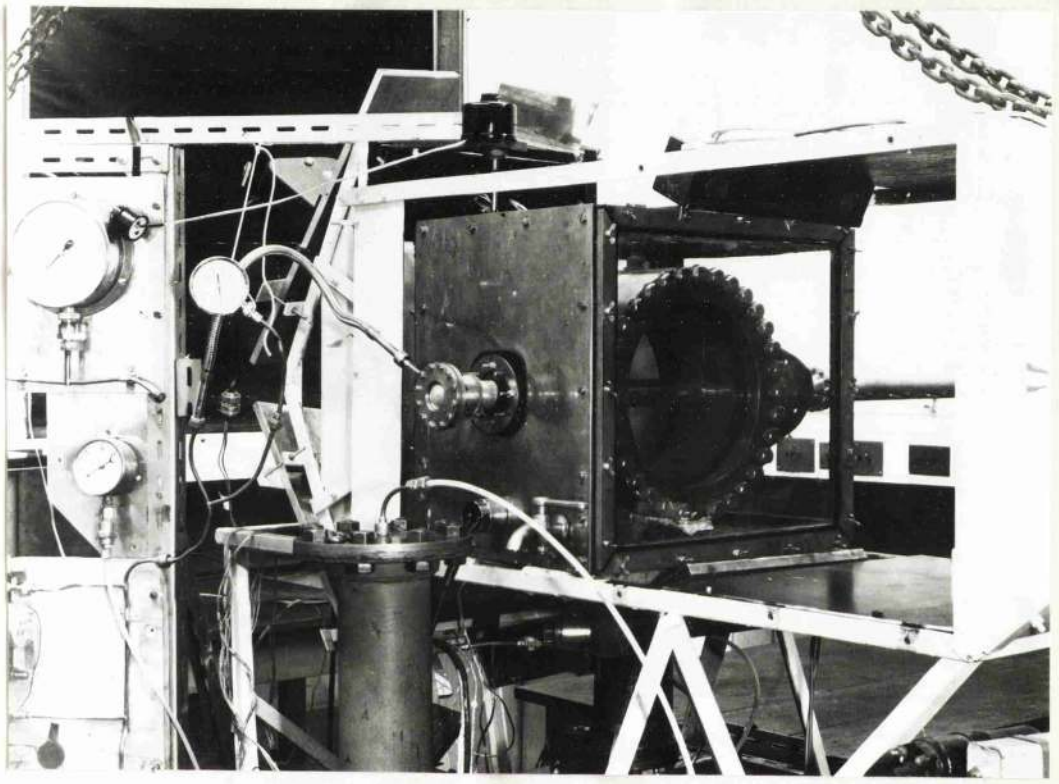

Fig.2a. A general view of the bubble chamber. The target tube can be seen passing through the chamber. The beam entry window is situated at the end of the extension tube on the right. The four cameras are behind on the left. The cylindrical lenses of the illuminating system have been removed to reveal the chamber.

controlled by a solenoidally operated, two way , Barksdale valve.

For one valve position, compressed air at 30 atmospheres is fed to the lower surface of the piston. The initial propane liquid - vapour mixture at its saturated vapour pressure of 20 atmospheres is thus completely liquified, the amount of propane being adjusted to give, for complete compression, a pressure in the chamber of 22 atmospheres. Switching the valve allows the compressed air in contact with the piston to exhaust to atmosphere and as a result the pressure of the propane forces the piston down. The sudden increase of the chamber volume reduces the still liquid propane to a pressure around 8 atmospheres below the saturated vapour pressure. The propane is thus in a sensitive superheated state until the pressure returns to the saturated vapour pressure under the influence of wall boiling.

Initially, the sensitive conditions of the chamber were determined using a Co^{60} source. γ-radiation from the source produces Compton electrons of energies up to 1,3 mev corresponding to a track length in propane of about 1 cm. The effects of varying expansion ratios and operating temperatures were examined.

The tests showed that sensitivity was just obtained with an expansion ratio of 1,4% at an operating temperature of 55°C. This was, however, minimum sensitivity, only the track ends being visible. Minimum ionising particles were not detected.

To observe the 1 cm. electron tracks completely an expansion ratio of 1,8% was necessary at an operating temperature of 61 °C. The increase of expansion ratio to values as high as 8% resulted in no appreciable increase of sensitivity . These conclusions were confirmed for longer tracks produced from targets placed in a high energy photon beam.

Fig. 3. shows the form of the pressure variation as measured with a commercial pressure transducer using a 2% expansion ratio. The time of travel of the piston was measured, using electrical contacts, to be $\sim$ 6 ms, the precise time depending on the condition of the piston seals. Expansion resulted in a minimum pressure of 12 atmospheres. The sensitive time of the chamber is of the order of a few milliseconds as shown by variation of the timing of the expansion relative to the arrival of a pulsed photon beam at the chamber. The optimum conditions for track formation occured between 0 and 1 ms after completion of the

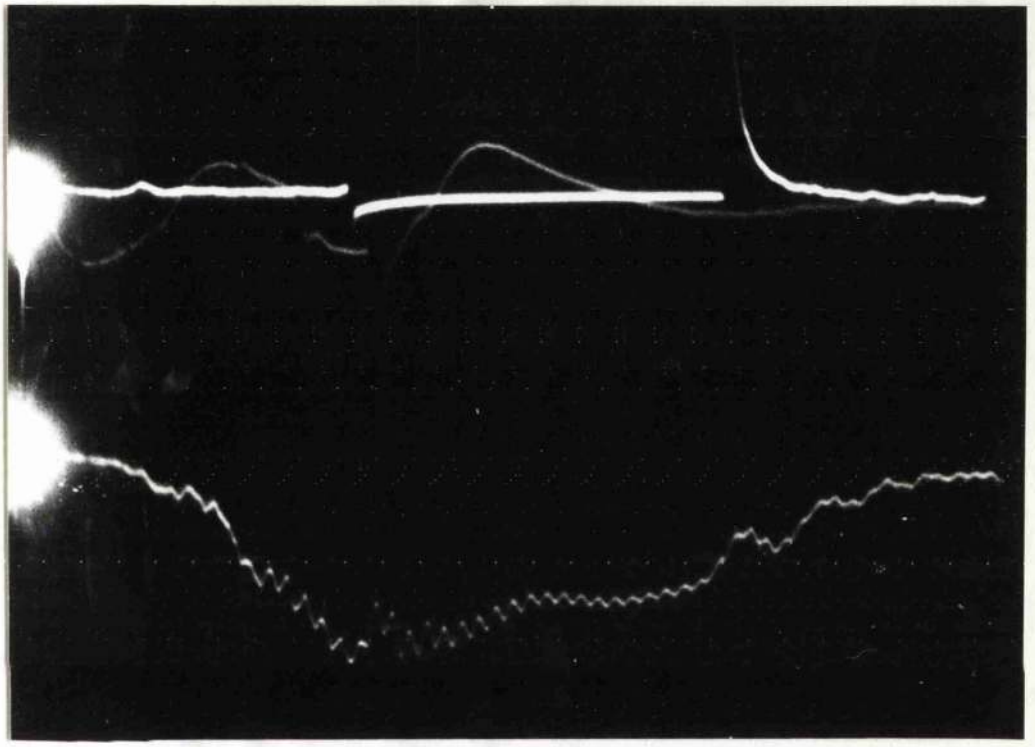

Fig.3. The lower trace shows the variation of pressure in the chamber from an initial value of 22 atm. to a minimum of 12 atm. in 6 milliseconds. Oscillations on the trace result from temporary positioning of the transducer head during the experiment. The upper heavy trace shows a negative pulse indicating complete expansion followed by a positive pulse 10 ms. later indicating the start of recompression. The upper faint trace shows a negative pulse corresponding to arrival of the photon beam 1/2 ms. after complete expansion.

expansion. The bubbles produced by ionising particles reach a sufficient size for photography in 1,5 - 2 ms after the passage of the particles.

The expansion ratio of 2% was chosen for operation as being the lowest practical value giving consistent operation of the chamber. Though a larger expansion ratio tends to give a longer sensitive time the smaller expansion ratio has two advantages. Large expansion ratios tend to create a greater disturbance in the chamber thus increasing the chances of track distortion. Further, a larger volume of vapour is released from wall boiling resulting in increased difficulty during recompression and the increased piston movement results in a greater consumption of compressed air during each expansion.

It is important in the operation of a bubble chamber to obtain as fast a cycling rate as possible when in the present case the synchrotron produces bremsstrahlung at a frequency of 250 pulses/minute. The cycling rate of a bubble chamber depends on the rate at which re-:compression takes place. The rate of recompression, in turn, depends on the rate of transfer of latent heat from the vapour to the liquid. This can be increased by increasing the pressure in the chamber, but a great increase in the rate of compression is obtained if the

bubbles can be completely recompressed before they are able to coalesce at the top of the chamber, since in this case the surface area available for heat transfer is much greater.

Aided by using the minimum expansion ratio, fast recompression is obtained by recommencing the recompression 15 ms after completion of the expansion. A 7,5 litre reservoir cylinder close to the Barksdale valve prevents any pressure drop of the air supply during recompression due to the impedance of the supply lines. The compressed air is supplied from a compressor of free air capacity of 5,7 litre sec^{-1} and enables a cycling rate of 30 expansions per minute to be maintained.

When the chamber is cycled for several minutes at 30 expansions per minute the chamber sensitivity is found to decrease slightly from its value for the first few cycles reaching a steady value after some 50 expansions. This results from the minimum pressure reached becoming nearly half an atmosphere higher. This change is accompanied by a rise of temperature in the chamber of about $1^{o}C$, resulting from the work being done on the propane. A compensation piston is used to control the variation of the pressure of the compressed propane arising from this temperature change.

In experiments performed with a photon beam one of the main difficulties is caused by the considerable electron background originating in the target. In the present case where a pure hydrogen target is used this background is nearly a minimum for most energies of electrons. However, it is still a serious limitation.

During the experiment, therefore, the chamber was operated at a temperature of 58,7°C. This temperature reduces the sensitivity to the minimum ionising electron tracks producing a decrease in the density of the background. This temperature is still sufficient to give good density pion and proton tracks and causes pions and protons to stand out from the electron background.

3. Photography and Illumination.

Four cameras are used to give stereoscopic photography since only with this number of cameras can a sufficient region of the chamber be observed. The position of the target tube in the centre of the chamber would otherwise exclude large regions of the chamber from view.

The cameras use Beattie magazines and hold 100 ft. of 35 mm. film, sufficient for 1,000 frames. The magazines are held behind shutterless lenses the exposures being controlled by the illumination.

The cameras are arranged in pairs, an upper and lower pair, the members of a pair subtending a stereo angle of 25° at the chamber. The pairs are separated with an angle of 40° (see fig. 4). The wider separation of the cameras in the vertical direction allows a greater coverage of regions otherwise hidden by the target tube.

Figure 4 indicates the illumination system and the arrangement of the cameras. The light source is an externally triggered tubular flash tube placed parallel to the target tube. The tube operates at 1,6 KV and dissipates 16 joules per flash, sufficient for use with R.55 film.

Dark field illumination is obtained by arranging the

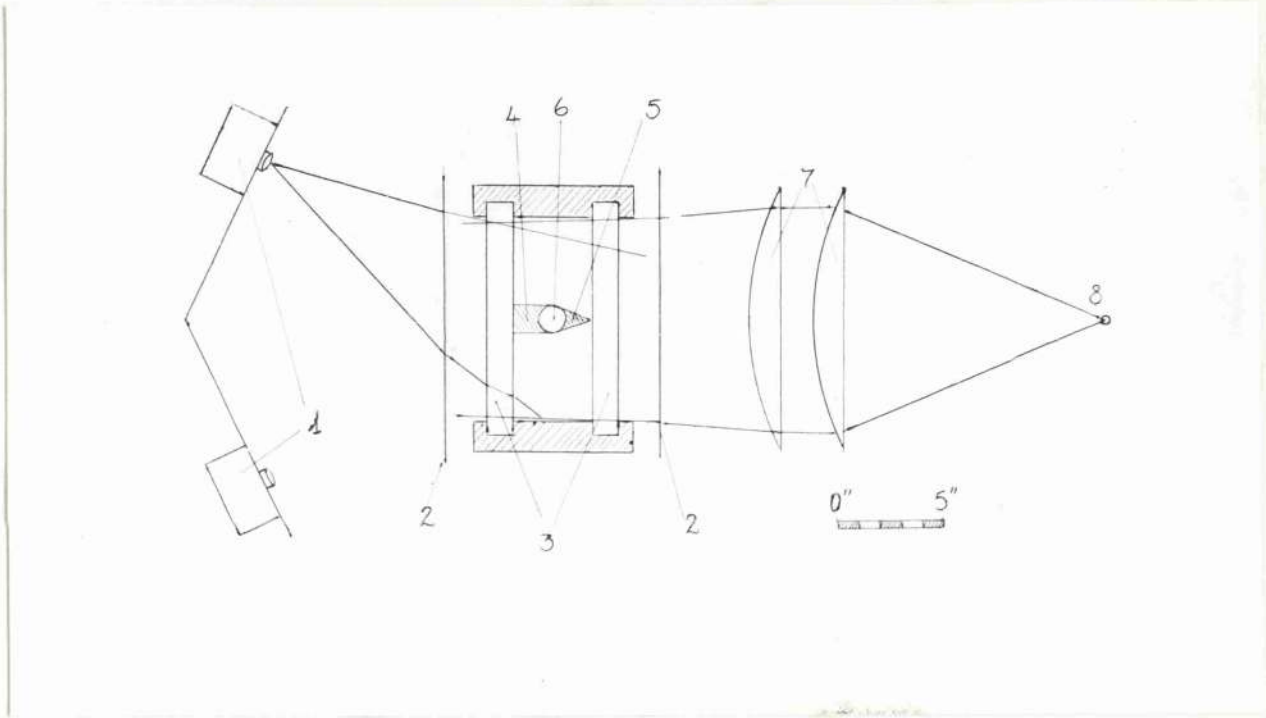

Fig.4. The Bubble Chamber optical system. 1. Cameras. 2. Windows of the water bath. 3. Chamber windows. 4. Volume of chamber not illuminated. 5. Volume of chamber not visible to the cameras. 6. Target tube . 7. Cylindrical light collimating lenses. 8. Flash tube light source.

light source to be not directly visible by the cameras. A fairly low scattering angle for light scattered from the bubbles into the cameras has been used since the intensity of scattered light decreases at larger angles (Davis,1955). At the mean scattering angle used, 30°, the scattered intensity is almost 25 times that at 90°.

Cylindrical lenses have been added to the lighting system to make the scattering angle more uniform throughout the chamber, since if the scattering angle varies appreciably the contrast is not uniformly good throughout the chamber. With the cylindrical lenses in place the scattering angle varies between 16° and 32° corresponding to a factor two in scattered intensity.

The cameras give a magnification of 1/10 and the lenses were stopped down to $f/16$. With these settings an adequate depth of field for the chamber is obtained and the recorded bubble images correspond to a diameter of 0,3 mm in object space.

4. The Experimental Lay-out.

The arrangement of the experiment is shown in fig. 5 . The collimation must allow sufficient clearance between the photon beam and the walls of the target tube through which it is passed in order to avoid background events occuring in the tube walls or the propane. Since collimation does not produce sharp limits of beam diameter the clearance must be generous.

The chamber was lined up to the beam using X-ray films exposed to the beam behind a 1/16" thickness of aluminium to indicate the beam position. Crosswires, temporarily located at the ends of the target tube also showed on the X-ray films thus indicating the position of the chamber relative to the beam.

The first collimator shown in fig. 5 limits the beam diameter. Initially a 3/16" diameter collimator, producing an 0,9" diameter beam at the chamber, was tried. Although the geometrical clearance is 0,25" considerable electron background was observed. Consequently a 1/8" collimator giving a beam diameter of 0,55" at the chamber was used and proved to be satisfactory.

The main problem in using a bubble chamber with a photon beam is to reduce the electron background, since this can limit the minimum particle energy detectable and

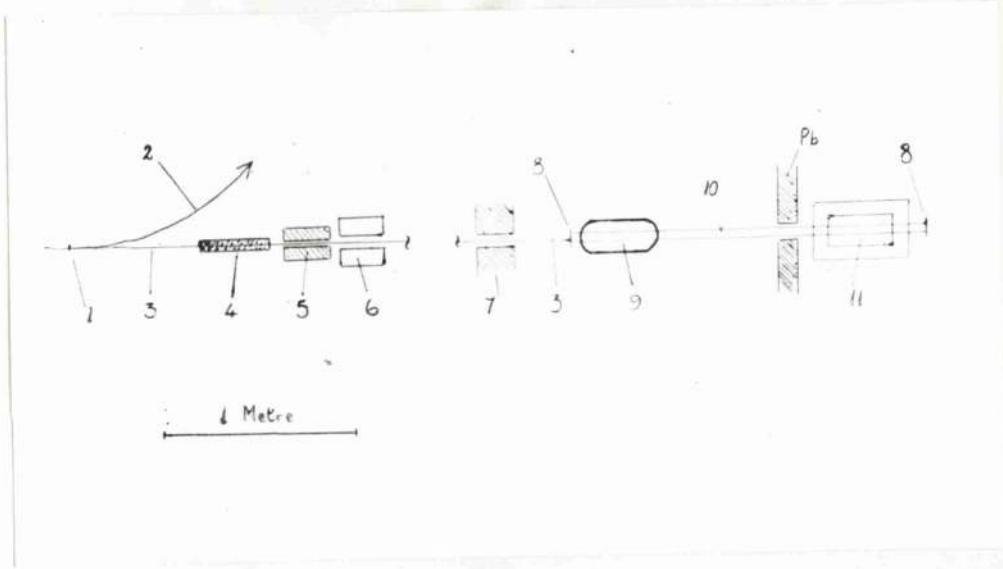

Fig 5. Schematic diagram of the layout of the experiment. 1. Synchrotron target. 2. Path of circulating electrons. 3. Photon beam. 4. Polythene beam hardener. 5. 1/8" diam. lead collimator. 6. Beam scrubbing magnet. 7. Second lead collimator. 8. Beam entry and exit windows of 40 thou. Milar. 9.Second scrubbing magnet. 10. Extension of the target tube. 11. The Bubble Chamber.

does limit the beam flux that can be accepted.

The use of a lower operating temperature to reduce the effect of background electrons, is only a partial solution. It is still important to keep the number of electrons entering the chamber to a minimum.

The electron background is produced in the hydrogen target itself and also arises in the 0,1 gm.cm^{-2} thick milar window (40 thou) through which the photon beam enters the target tube. The electron background from the beam entry window is comparable with that from 50 cm. of hydrogen and thus contributes considerably to the background in the chamber if the beam window is close to the chamber. A reduction of the background was achieved by extending the target tube to place the beam entry window in the field of a sweeping magnet 125 cm. from the chamber. Electrons produced in the beam entry window were deflected out of the beam and although an extra thickness of hydrogen was introduced before the chamber a net reduction of electron background in the chamber was obtained.

With the target tube evacuated the electron background observed in the chamber was neglegible indicating the hydrogen as the sole source of background.

The majority of background electrons are produced by low energy photons. Beam hardening has been used

to reduce the number of low energy photons in the beam relative to those of greater energy.

16" of polythene hardener was placed before the first collimator, producing a relative decrease in the number of photons below 25 mev. The attenuation above 100 mev is roughly constant at 0,6 but since the chamber can only accept a small beam intensity this attenuation is not important.

After passing through the hardener and first collimator, the beam passes through a scrubbing magnetic which removes electrons produced at the collimator and hardner from the beam. A second lead collimator does not directly collimate the beam but is arranged to cut down photons scattered from the first collimator which would otherwise reach the walls of the target tube. A final lead wall was placed immediately in front of the chamber and cut down the few electrons entering the chamber through the walls.

Under these conditions the background in the chamber with the target tube evacuated was negligible, amounting only to a few electron tracks per beam, with beam intensity of 2.10^5 equivalent quanta per pulse. During the experiment the target tube contained hydrogen at a pressure of 42 atmospheres when the electron background arising in the hydrogen limited the γ-beam intensity that could be

used to 2,5. 10^5 equivalent quanta per pulse. This background consists of relatively short and predominantly forward tracks concentrated within a few centimetres from the tube. Nevertheless it is usually possible to trace tracks of pions or protons to within 1 cm. of the tube. Detection of pions or photons with track length much less than 2 cm. in propane is too difficult to be reliable.

The background therefore as well as limiting the beam intensity that can be used also determines the minimum particle energies that can be detected as shown below.

TABLE - Minimum Energy (lab) for Detection.

	30°	60°	90° (lab angles)
π	17,2 mev.	15,8 mev.	15,6 mev.
p	40.6 mev.	37.2 mev.	36,6 mev.

5. The Operation of the Chamber.

The synchronisation between the expansion of the chamber and the production of the photon beam is obtained by use of a timing pulse received 80 ms. before the arrival of the beam at the chamber. This timing pulse is fed through a gate circuit which permits the passage of only one timing pulse, the passage of the pulse causing the gate to close. The gate is opened by a control pulse which is produced at a frequency corresponding to the desired cycling rate of the chamber.

Thus though timing pulses are received with frequency 250/min, only a few are accepted at a rate suitable for chamber operation. The accepted timing pulses are suitably delayed in a phantastron type circuit, with a stability better than 0,1 ms. The delayed pulse is responsible for operation of the Barksdale valve and consequent expansion of the chamber.

An oscilloscope display of the pressure trace and a pulse synchronous with the photon beam is used to give approximate adjustment of the timing (see fig. 3). A more accurate adjustment makes use of a pulse produced at the moment of complete expansion. This pulse is produced when, on complete expansion, the piston connects two electrical contacts mounted in the piston housing.

During chamber operation an oscilloscope displayed the beam pulse and a pulse obtained from a photocell recording the illumination. The trace was triggered on the pulse produced at complete expansion.

The beam was received 1 ms. after completion of the expansion and the flash lamps were fired 1,8 ms. later. The cycling rate during the experiment was 20 - 25 cycles per minute enabling one roll of film containing 1000 frames to be taken per hour. At any time it was possible to take a single photograph with a "Polaroid" camera. This camera gave a finished print one minute after exposure and was used to monitor the sensitivity of the chamber.

6. The Analysis of the Events.

Study of the event

$$\gamma + p \rightarrow \pi^{+} + n$$

involves determination of the direction and length of the pion track by the combination of measurements from two or more views of the event.

Cloud chamber pictures have been analysed by reprojective stereo pairs through a system optically equivalent to that through which the photographs were originally taken. The position in which the two projections of a given track coincide indicates the spatial position of that track. This method is not so convenient in the present case, since liquid propane has a refractive index of 1,3.

Measurements have, therefore, been made on individual photographs and combined with those from other photographs of the same event to give data for the computation of the spatial positions of the tracks.

The measurements are made relative to reference marks placed on the inner surfaces of both windows. Fig. 6 shows the position of the cameras relative to the chamber and the coordinate system used to describe events in the chamber. The reference marks, shown in the diagram on one window only, are at known positions relative to the

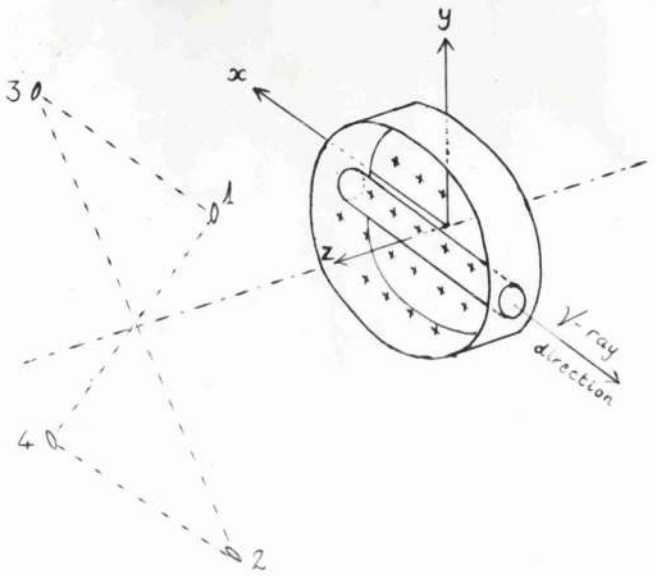

Fig.6. A schematic representation showing the camera positions 1,2,3,and 4 relative to the chamber. The co-ordinate system x,y,z used in the analysis of tracks is also indicated. Reference marks (+) are shown on the front window, those on the rear window are not shown.

chamber coordinate system. The surfaces on which the reference marks appear correspond to the planes $Z=0$ (rear) and $Z=d$ (front.)

Consider, for example, the end point of a track Q with coordinates x, y, z as shown in figure 7. Light from this point reaches a given camera by travelling in the appropriate direction in the chamber. The path taken by the light is a straight line passing through Q and intercepting the inner window surfaces at x_F, y_F, d and $x_B, y_B, 0$ say. Obviously when looking at the photograph these three points will appear coincident. Thus each point on a photograph corresponds to a straight line in the chamber. Since the reference marks lie on the planes $Z=0$ and $Z=d$ measurement relative to the reference points leads to the coordinates x_F', y_F', d and $x_B', y_B', 0$ defining the line on which the measured point lies.

In practice the photographs are projected at $1\frac{1}{2}$ times life size onto a scanning table. For each view a graph paper sheet is lined up with the reference marks and gives a coordinate system ξ, η in terms of which measurements are made on the photographs.

The reference marks are placed at known positions x_i, y_i, d and x_j, y_j, d for front and rear

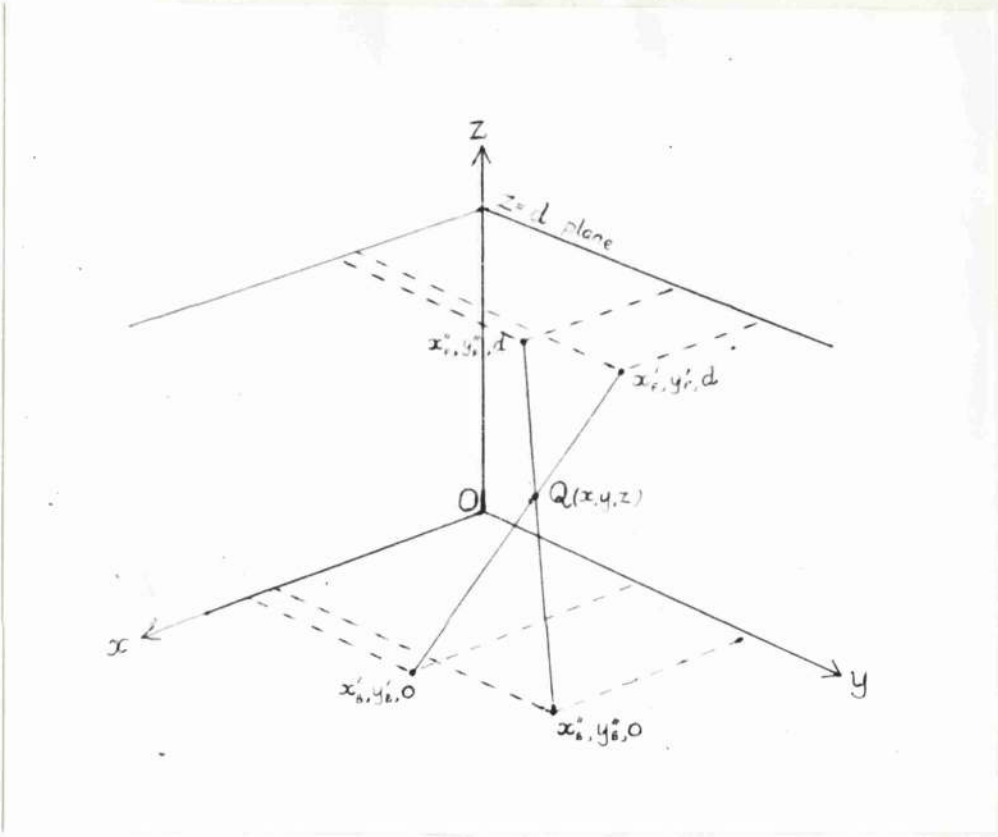

Fig.7. The diagram illustrates the method for the determination of the spatial position of the track end-point Q. See text for explanation.

windows respectively. Measurement of their positions in each view relative to the axes ξ, η relates the coordinate system to the chamber coordinates x, y, z. Thus the measurement in one view of the ξ', η' coordinates corresponding to a given point on a track determines the coordinates x_F', y_F', d and $x_B', y_B', 0$ which define the line on which the measured point lies. The relationship between the coordinate systems was found to be fitted by equations of the form

$$x = A + B\xi + C\xi^2 + D\eta + E\eta\xi$$
$$y = A' + B'\eta + C'\eta^2 + D'\xi + E'\xi\eta \qquad (38)$$

In the case of measurement of the end point of a track, or a point of interaction, the identical point is measured in the different views. The measurements lead to two or more lines on which the measured point lies and the intersection of these lines gives the spatial position of the point.

However in general a point on a track measured in one view cannot be exactly identified in another. In the measurement of π^+ tracks in the present experiment, only the end point of the track allows measurement of the corresponding points of the track in all views.

When corresponding points in the different views cannot be measured two or more points, measured in a given view along the track, essentially define a plane in which the track lies, in a way analogons to a single measurement defining a line on which the measured point lies. The intersection of planes determined from two views gives the spatial position of the track.

The first clearly visible point of the track, ξ_P', η_P' was measured together with a further point ξ_μ', η_μ', so defining the track direction in the view measured. As before each of these points represents a line in the chamber corresponding to the ray path taken by light from the observed point to reach the camera considered.

The Equations (38) give the points P_F', P_B' and U_F', U_B' as defining the lines corresponding to ξ_P', η_P' and ξ_μ', η_μ'. This is shown in figure 8. The points P_F', P_B', U_F', U_B' define the plane containing the length of track PU. In a similar way measurement on a second view leads to points P_F'', P_B'', U_F'' and U_B'' which do not usually correspond to the points P and U on the track.

We see from the diagram that the line $P_F' U_F'$ cuts the line $P_F'' U_F''$ at X_F, Y_F, d which lies on the line PU. Similarly X_B, Y_B, o is given by the intersection of $U_B' P_B'$ with $U_B'' P_B''$.

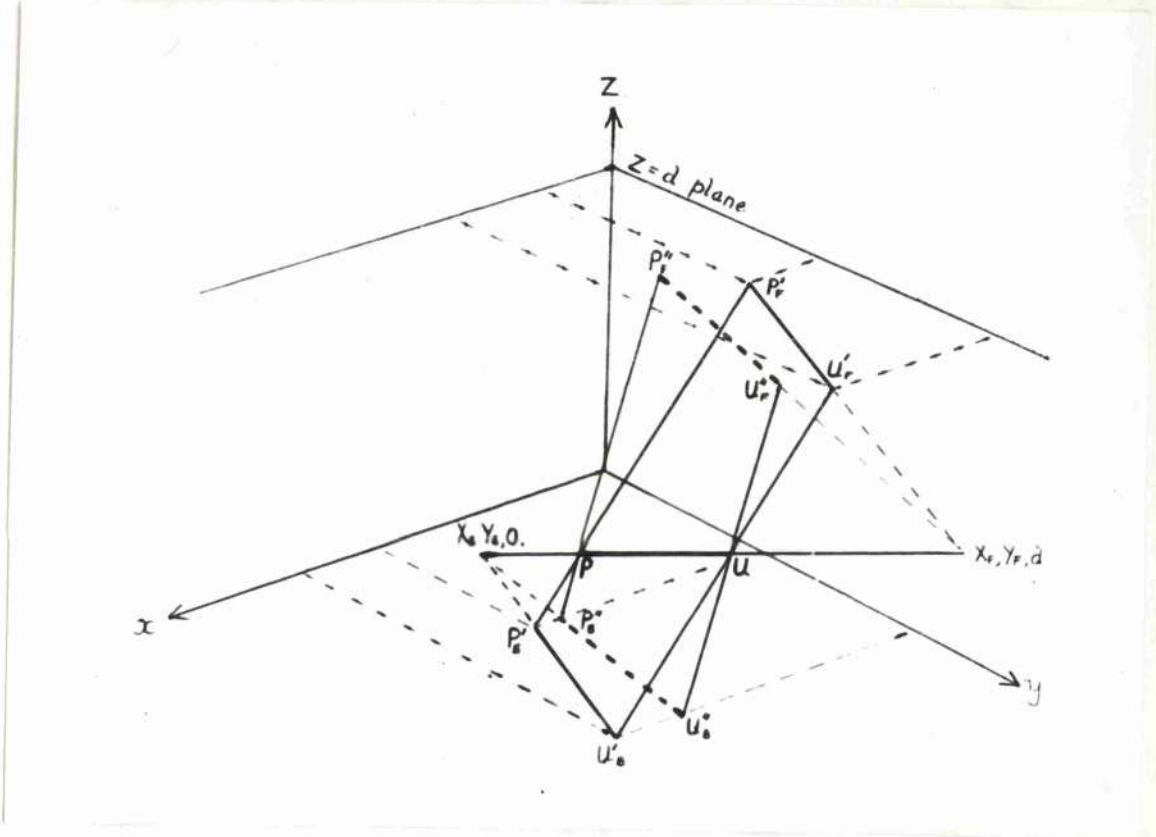

Fig.8. The diagram illustrates the method used to determine the direction cosines of the tracks l,m,n. See text for explanation.

Thus the track in the region between the points P and U has direction cosines

$$l \propto (X_F - X_B) \qquad m \propto (Y_F - Y_B) \qquad n \propto d$$

and its position in the chamber is determined.

The photographs of events are treated in pairs. When a choice is possible, the pairing of the views is chosen so as to give the largest angle between the planes whose line of intersection determines the track direction. This requires use of a camera pair such that the line joining the cameras is more or less perpendicular to the track direction viewed on the photographs. The choice of camera pairing does not affect the accuracy of the determination of the track end point, Q.

In practice the two lines whose intersection determines the position of Q do not intersect exactly. If the separation between the lines was more than 0,1" the event was remeasured.

Since the tracks measured are practically straight, the point Q ought to lie on the line joining X_F, Y_F, d and $X_B, Y_B, 0$. However if the direction cosine n is very small this is not necessarily the case because of the large distance of X_F, Y_F, d and $X_B, Y_B, 0$ from Q in this case. The tracks have therefore been taken as the line through

x_Q, y_Q, z_Q with direction cosines l, m, n .

The computation is done using a Dence computor. The initial measurements were fed in on punched cards, values of the end point positions, direction cosines and particle energy were determined. The distance S_Q of the end point from the line joining x_F, y_F, d and $x_B, y_B, 0$ was also computed. This gives a check on the calculation of l, m, n . The value of S_Q should be small except when $n \rightarrow 0$. A further check of direction cosines is given by determination the closeness of the extended track to the axis of the target tube. Events giving unreasonable values were reanalysed.

In about 40% of the tracks observed measurements could be made on four cameras, thus allowing two independent calculations of track end point position and track direction, to be made. From a comparison of these measurements it is possible to deduce the accuracy of measurement resulting from random errors in measurement of the events and location of the reference marks.

Comparison of these measurements indicates the following errors

	Camera Combinations	X_Q	Y_Q	Z_Q	ϑ
$\perp$ tracks	(1,3)(2,4)	$\pm$,35 mm	$\pm$,80 mm	1,1 mm	1,5°
// tracks	(1,2)(3,4)	$\pm$,80 mm	$\pm$,35 mm	1,1 mm	3,0° *

* at 30°

The programme calculates for each track the value Sc, which is defined as the closest distance of the track to the tube axis, when extrapolated back into the target tube. Fig.9 shows the distribution of Sc for 443 computed pion tracks.

In the case of exact measurement of the tracks the distribution should depend only on the characteristics of the photon beam.

Let the flux in the beam at distance τ from the beam axis be

$I(\tau)$ photons/cm^2

or $I(\alpha,\beta)$ photons/cm^2 when written in Cartesian coordinates. Then the distribution of Sc has the shape

$$N(S_c)\,dS_c \propto \int_{\beta=-\infty}^{+\infty} I(\alpha = S_c, \beta)\,d\beta\,dS_c \qquad (39)$$

The observed distribution of Sc is very closely Gaussian with a standard deviation 0,70 cm whereas the

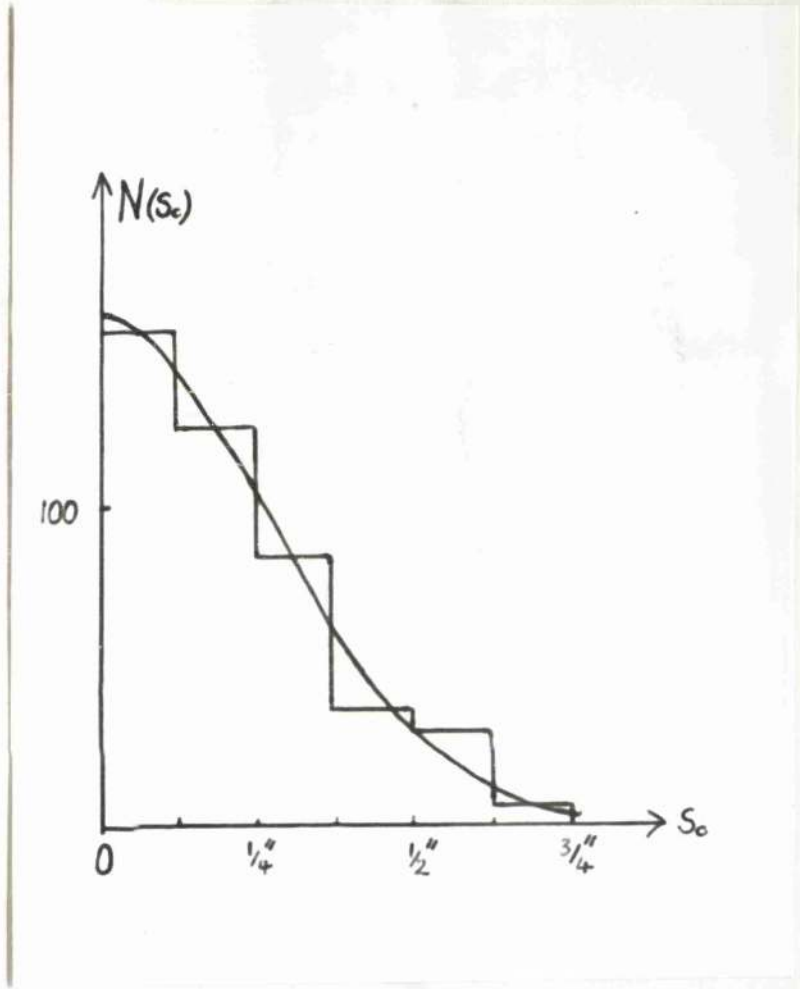

Fig.9. The observed distribution of S_c values is shown as a histogram. The smooth curve shows the Gaussian giving the best fit.

geometrical beam radius is 0,65 cm. This large difference is due to the errors of analysis appearing in the value of Sc.

Because of the chamber geometry, the majority of tracks lie close to the x, y plane. For 70% of the tracks the direction cosine $n < 0,5$. As a result the error in Sc arises mainly from combination of the errors in Z_Q and n which are $\pm$ 0,11 cm. and $\pm$ .05 respectively. This gives an error of $\pm$ 0,4 cm in the value of Sc for an average track produced at 90°. Combining this with the distribution (39) above, which can be approximated to a Gaussian of deviation 0,3 cm, we expect a distribution, nearly Gaussian, with standard deviation $\pm$ 0,50 cm.

This value is to be compared with the observed value $\pm$ 0,70 cm. This difference is expected since for tracks at angles different from 90° the expected error in Sc will be larger. Taking this into account gives a standard deviation 0,65 cm.

The distribution of track origins is thus consistent with the calculated accuracy of the analysis and the dimensions of the beam at the chamber and is therefore evidence that the observed tracks originate from the region of the target traversed by the photon

beam.

The observed distribution is compared with the Gaussian of deviation 0,70 cm in the following table. The distribution is given in 6 intervals 1/8" wide.

							Sc	3/4"
observed distribution	156	126	85	37	31	8	-	
calculated distribution	155	127	85	45	21	7	3	

IV. The Photoproduction of π^+ from Hydrogen.

1. Selection of the Events.

40 000 photographs, 4 views for each of 10 000 expansions, were scanned for pion tracks. The films were scanned directly under low magnification (x 5), the four corresponding frames being scanned simultaneously.

Since, in a bubble chamber not having an accurately controlled final pressure, bubble density measurements are not reliable, the pion energy must be determined from range-energy relationships. Thus only pions which stop in the chamber are of interest. Consequently, the pions were principally identified by the characteristic $\pi - \mu$ decay, a pion decay at rest producing a muon track of length 0,29 cm. in propane. Qualitative observation of multiple scattering and the variation of bubble density along the track also gives a useful guide to track identification. Photographs of a pion track showing the $\pi - \mu$ decay and a proton track are shown in figures 10 and 11 respectively.

Tracks with multiple scattering and bubble densities appropriate to pions were also observed without a $\pi - \mu$ decay. These events were also measured and the analysis confirmed the conclusion that these tracks left the chamber.

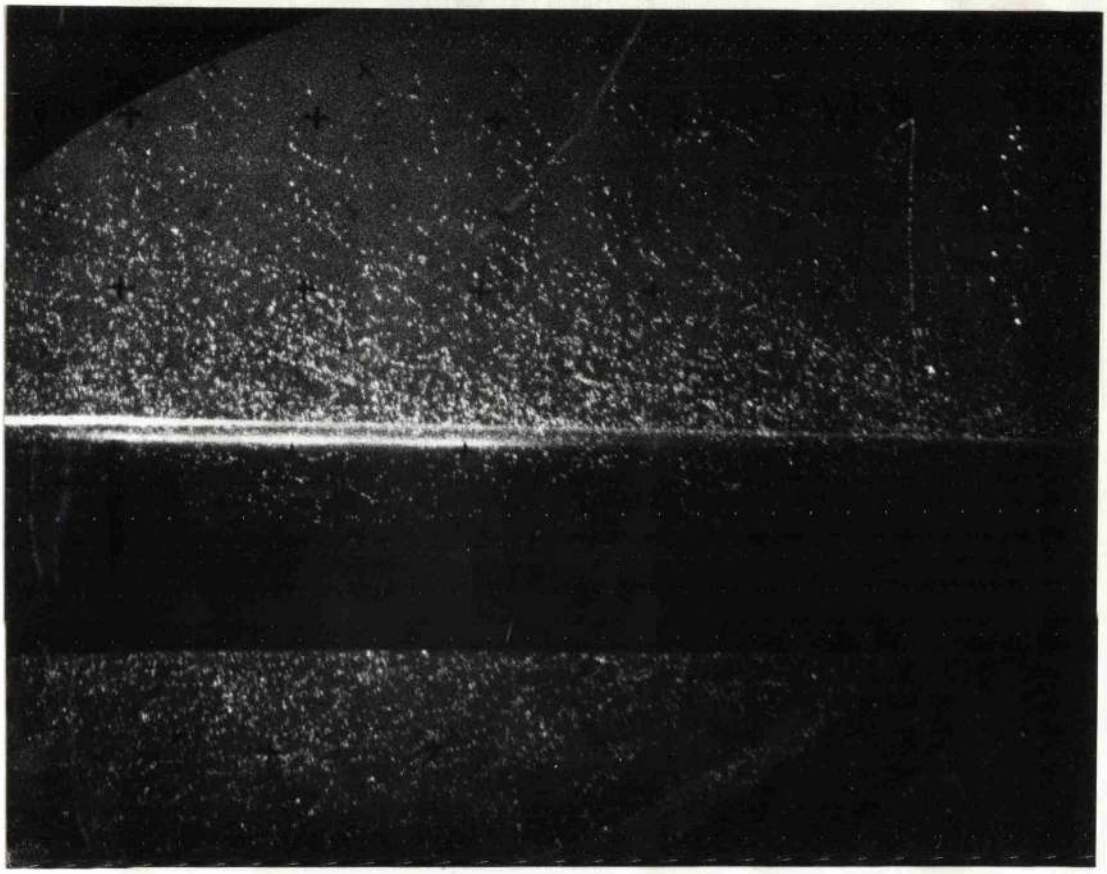

Fig.10. The Bubble Chamber photograph shows a Pion which is identifiable by the decay into a Mu-meson. The chamber sensitivity is too low for the decay electron to be easily visible..

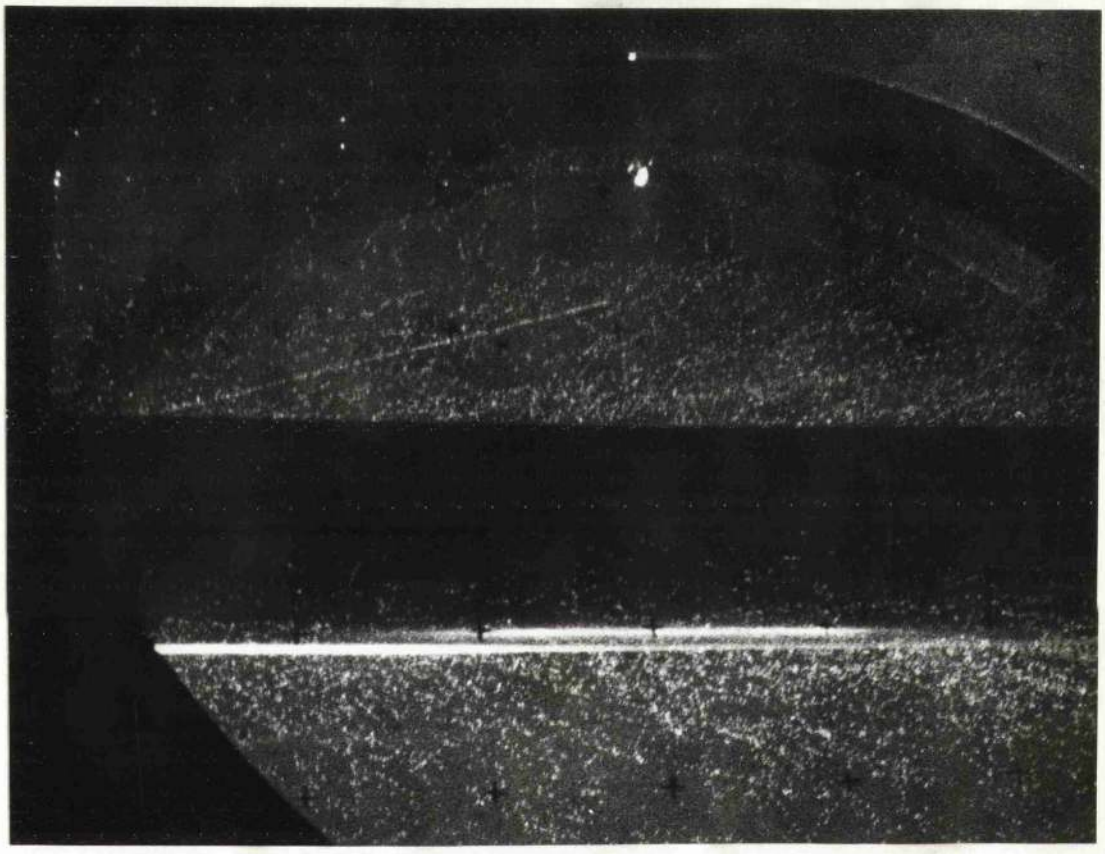

Fig. 11. A Bubble Chamber photograph of a proton track. Proton tracks have a higher bubble density and are noticably straighter than the pion tracks.

Some 1000 pion tracks were measured in the manner indicated in the previous chapter. 455 pions were found stopping in the chamber, 383 of which lay in the range corresponding to photon energies E_γ = 165 - 211,5 Mev. 72 events, corresponding to photon energies greater than 211,5 Mev were not included in the analysis since they are observed only at very backward angles and the statistics are relatively poor.

Pions were accepted for inclusion in the results from the angular range 15° - 165° in laboratory coordinates. Additional criteria were also used to define an accepted event.

To avoid including tracks which have interacted in the chamber walls, accepted pions were required to leave the target tube at a distance from the chamber walls greater than 1/4", that is, from a section of the target tube 24,13 cms. in length. These limits on the point of entry of acceptable pions into the chamber define the thickness of the hydrogen target available. Although accepted pions may be produced in the hydrogen at points beyond these limits in the case of particles not emitted at 90°, the effective target thickness for all production angles is 24,13 cms. corresponding to 0,075 gm/cm^2 hydrogen

at 42 atmospheres and 58,7°C. The temperature of the target is taken to be the same as that of the bubble chamber measurements showing the difference to be less than ½ °C.

A further requirement is imposed to eliminate very short tracks which are both difficult to identify and to find during scanning. The accepted tracks were essentially required to show a visible length greater than 2 cm. when projected into a plane parallel to that of the film. In other words, the track length appearing on the film must exceed the minimum acceptable value .

In practice, to facilitate the calculations of geometric detection efficiency for the chamber the tracks are required to end at least $T_{lim} \sin \theta$ centimetres, measured in the y - direction (see fig. 6 page 62) beyond the boundary of the unobservable regions of the chamber, where θ is the angle of the track relative to the tube axis and T_{lim} is chosen equal to 2 cm. T_{lim} represents the length of visible track on projection into the xy - plane.

The unobservable regions of the chamber are shown in fig. 4 and are a direct consequence of the presence of the target tube in the chamber. These unobservable regions, one hidden from the cameras by the tube and the

other not illuminated are well defined since they depend solely on the position and dimensions of the tube. Their boundaries have been determined for use in the geometrical efficiency calculations. The boundaries of the region not visible to the cameras were determined directly from measurements on the films. The unilluminated region was determined from the relative positions of the light source and the target tube.

For the reasons indicated above, the accepted pions must enter the chamber from a region of the tube 24,13 cm long, corresponding to an effective target thickness of 0,075 gm. hydrogen per cm^2. However, not all pions satisfying this condition both show a sufficient track length and stop in the chamber. The geometric efficiency of the chamber for tracks of given production angle and range R is the fraction of tracks of accepted origin which both stop in the chamber and show sufficient track length. The geometric efficiency was computed as a function of θ , the production angle in the laboratory system, and r , theperpendicular distance of the track and point from the wall of the target containing tube.

The events were corrected individually for the geometric efficiency before being placed into the appropriate energy-angle intervals. The errors on the

computed values of α and τ give rise to uncertainties in the efficiency factors which contribute to the errors of the corrected yield values. This error contribution becomes increasingly large for tracks for which the chamber efficiency is low. The inclusion of a few tracks with low detection efficiencies in some energy-angle interval would contribute a large error. Thus a final condition for an accepted event is the requirement of a detection efficiency not less than 20%.

With this condition, the uncertainties in the efficiency factor contribute only slightly to the total error compared with the statistical error. The error in the efficiency factor in the worst case is 10%, in most cases it is 2%. If the efficiency factor was uncertain by 10% for each event in some energy-angle interval, which is not the case in practice, the statistical error would be ten times the error resulting from uncertainty of efficiency. Thus for the accepted events the uncertainties in the efficiency factors contribute only a negligible effect to the total error.

Using the above conditions to define an accepted track the original 383 events in the photon energy range EY = 165 - 211,5 mev are reduced to 332 accepted events.

2. Background Events.

In a previous section, it has been shown that the region of origin of the pion tracks is consistent with all the pions being produced in the hydrogen and indicates the absence of a serious background from the walls of the target tube.

To obtain further information on possible background pions 1000 x 4 photographs were taken with the target containing tube evacuated. The satisfactory sensitivity of the chamber during this run is confirmed by the few electron tracks seen in each photograph. During these 1000 expansions two protons and no pions were observed. This small yield together with the considerable decrease in the number of electron tracks showed that interactions between the bremsstrahlung beam and the walls of the target tube or the propane is very small. The background production of pions from material other than contained in the tube appears negligible.

The last conclusion is confirmed by the runs with hydrogen. Any production of positive pions from the tube walls or propane would be accompanied by roughly equivalent numbers of negative pions. Only one negative pion was observed stopping in the chamber during the experiment.

Similarly, appreciable impurity in the hydrogen used to fill the target tube would be revealed by the production of a number of π^--mesons. The quoted impurity in the hydrogen used is 0,01%, the main impurity being nitrogen. This amount of nitrogen has a negligible effect on the pion yields. Consequently any background contribution to the π^+ yield is entirely negligible and no background correction has been made.

3. The Bremsstrahlung Beam.

Electrons accelerated to 320 mev in an electron synchrotron produced bremsstrahlung radiation at a tungsten wire target 60 thou. in diameter. The beam was monitored after passing through the hydrogen target by a Wilson type Quantameter (Wilson,1957). The beam flux was recorded continuously, the resulting curves being integrated to give the total number of equivalent quanta passing through the hydrogen target. Correction was made for the relatively slow cycling rate of the bubble chamber compared with the synchrotron repetition rate of 250 pulses per minute, assuming an average intensity for the beam-pulses observed by the bubble chamber.

$$\text{Observed Quanta} = \frac{\text{Recorded Quanta}}{250} \times \frac{\text{No of useful photographs on film}}{\text{Time (mins.) for exposure of film}}$$

The thin target spectrum calculated by Schiff(1951) has been used as a good approximation for a wall collimated beam since the majority of forward photons are produced in the first few thou. of the target before appreciable energy loss can occur.

Correction has been made for the 16" polythene beam hardener under the assumption that each interacting

photon is permanently removed from the beam. This assumes that the electrons resulting from photon absorption do not reradiate appreciably in the forward direction. Swanson et al.(1960) indicate that electrons are removed by multiple scattering before reradiation occurs and that high energy pairs do not produce significant forward radiation. Divergences from this assumption tend to favour a greater intensity for low energy photons at the expense of high energy photons but probably has least effect in the middle of the spectrum.

4. The Scanning Efficiency.

The scanning efficiency has been determined by rescanning the film for π^+ tracks. 2000 photographs have been rescanned and give a scanning efficiency very close to 100%. No further π^+ tracks stopping in the chamber were discovered during the rescan.

For the purposes of the calculation of scanning efficiency the accepted pions were divided into two groups corresponding to pion energies greater and less than 25 Mev. respectively. The scanning efficiencies of these two groups were then determined independantly to check for any dependance of scanning efficiency on track length. The scanning efficiencies for both groups were found to be better than 95% indicating a closely constant scanning efficiency for all the accepted pions.

Very short tracks were excluded from the analysis of the data since it is fairly certain that the scanning efficiency must decrease for very short tracks since they become difficult to distinguish in the dense electron background close to the tube. Only tracks for which T_{lim}, defined in section 1 of this chapter, is greater than 2 cm are therefore accepted. Justification of this limit is made by comparison of results obtained for the limits T_{lim} = 2cm with a calculation using T_{lim} =2,5cm and appropriate geometrical efficiency, as described in a following section.

5. Minor Corrections.

The width of the hydrogen target has a negligible effect on the energy resolution. For tracks produced at 20° the path length of a particle produced in the photon beam is uncertain by $\pm$,015 gm/cm^2, corresponding to an energy uncertainty of 0,2 mev for a 20 mev pion. At 90° ΔE = 0,05 mev for a 20 mev pion.

Corrections have been added for decays in flight of 1 - 3% and for absorption of π^+ mesons in propane of less than 1% from data for carbon given by Stork(1954).

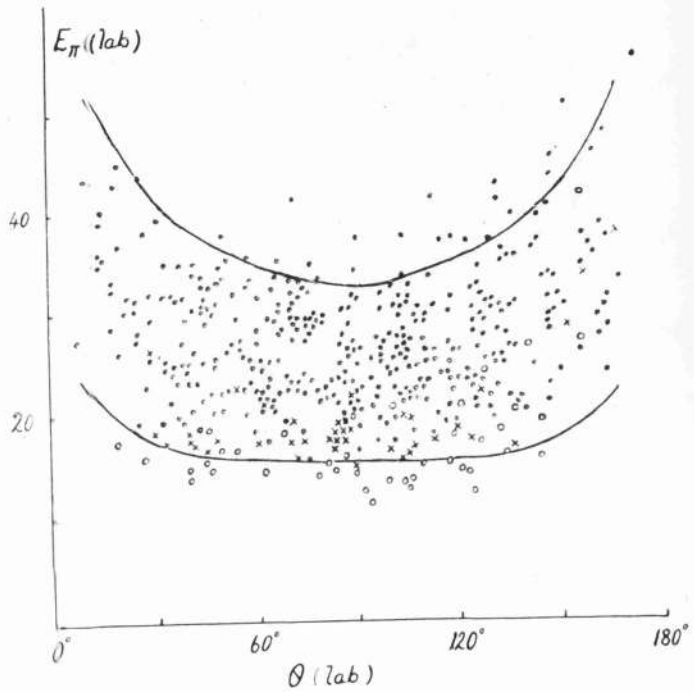

Fig.12. The plot shows the energy-angle distribution of the observed π^+. The solid lines correspond to a 20% geometrical detection efficiency. The open circles represent pions not accepted because of insufficient track length. Crosses represent pions for which $2{,}0 < T < 2{,}5$ cms.

6. Results.

All the observed pions are plotted in fig.12. where open circles refer to pions excluded from the analysis because of insufficient track length, The pions represented by crosses have track lengths corresponding to 2,0 cm $<$ T $<$ 2,5 cms. The two solid curves show the limits for which the chamber efficiency is 20% for T_{lim} = 2cm. The accepted events have been divided into five photon energy intervals and the centre of mass angular distributions are shown in fig.13 and tabulated in Table IV .

The best values for the differential cross sections at 90° C.M. have been obtained from curves fitted to the angular distributions. The angular distributions for the three lowest energy intervals have been fitted by least squares to a constant, a straight line and a quadratic respectively in terms of the variable Cos θ^*, where θ^* is the pion production angle in centre of mass coordinates (see fig.13). The differential cross section at 90° C.M. for the interval of mean photon energy 196,5 mev was determined with the guidance obtained by fitting the central three points to a constant and the best straight line. The highest energy interval required extrapolation to 90° from backward angles. This was

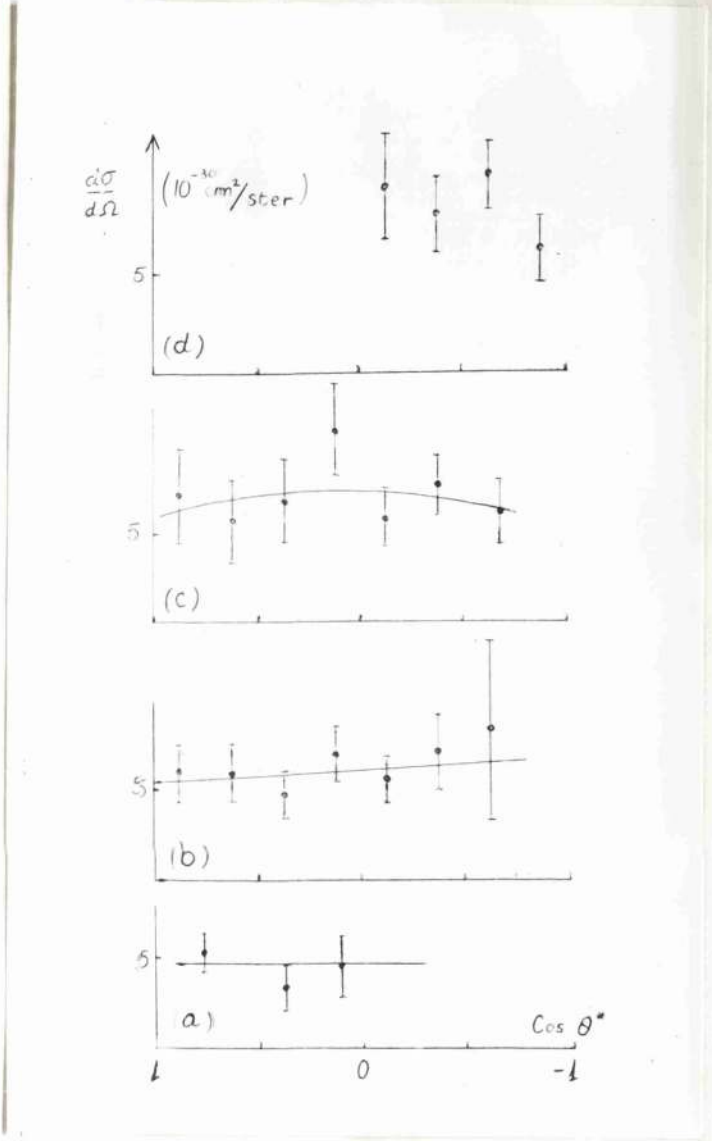

Fig.13. Angular distributions are shown for $\gamma + p \rightarrow \pi^+ + n$ for the energy intervals 165 - 173,5 Mev (a), 173,5 - 182,5 Mev (b), 182,5 - 191,5 Mev (c), and 191,5 - 201,5 Mev (d). The solid curves show least squares fits to the angular distributions. Standard deviations are shown.

Table IV.

$\frac{d\sigma}{d\Omega}$ $(\gamma+p \rightarrow \pi^{+}+n)$. (10^{-30} $cm.^2$/ sterad.)

E_γ (Mev).	Cosine θ^*							
	0.875	0.625	0.375	0.125	-0.125	-0.375	-0.625	-0.875
165 - 173.5		5.5 $\pm$1.1 *	3.5 $\pm$1.4	4.7 $\pm$1.8				
173.5 -182.5	6.2 $\pm$1.7	6.1 $\pm$1.7	4.9 $\pm$1.4	7.3 $\pm$1.6	5.7 $\pm$1.5	7.4 $\pm$2.2	8.6 $\pm$5.6	
182.5 -191.5	7.4 $\pm$2.8	5.9 $\pm$2.5	7.0 $\pm$2.3	11.1 $\pm$2.7	6.0 $\pm$1.7	7.9 $\pm$1.7	6.3 † $\pm$1.5	
191.5 -201.5					10.2 $\pm$3.4	8.5 $\pm$2.2	10.8 $\pm$2.1	6.4 $\pm$1.7
201.5 -211.5							9.6 $\pm$2.2	5.8 $\pm$1.6

* Cos $\theta^* = 0.75$

† Cos $\theta^* = -0.675$

done by eye and a large part of the error on the 90° cross section arises from the uncertainty involved in this proceedure.

The quantity

$$a_o^+ = |T^+(90^\circ)|^2 = \tfrac{1}{W} \frac{d\sigma}{d\Omega}(90^\circ \text{ C.M.})$$

where

$$W = q\, q_o \left(1 + \frac{k}{M}\right)^{-2}.$$

has been calculated from the 90° differential cross sections obtained from the angular distributions. The results are given in the following table.

Table III.

E_γ =	169.5	178.0	187.0	196.5	206.5	(Mev.)
a_o^+ = (cm./sterad.)	12.9 $\pm$2.1	13.7 $\pm$1.4	13.6 $\pm$1.8	14.o $\pm$2.1	13.0 $\pm$2.9	

and shown in figure 14.

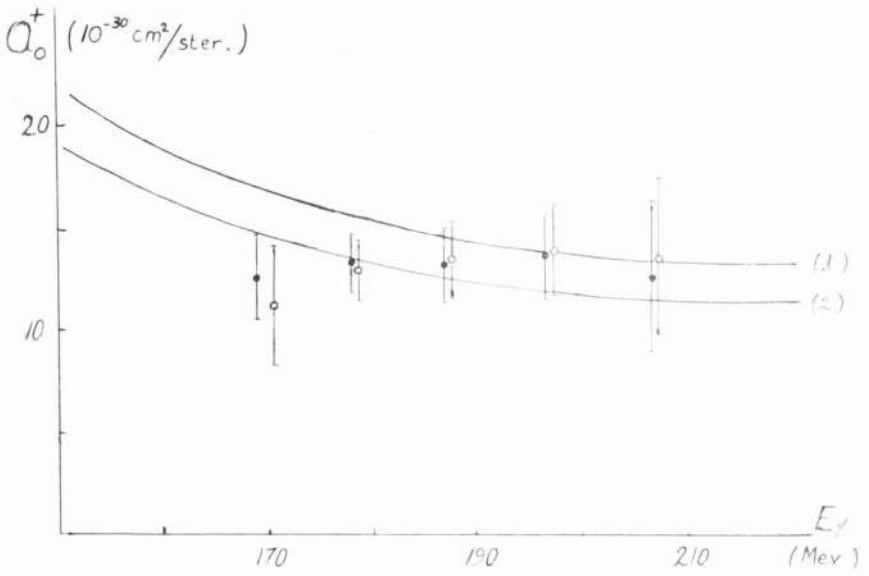

Fig.14. The values of a_o^+ obtained in the present work are shown for $T_{lim} = 2$ cm. (solid points) and $T_{lim} = 2{,}5$ cm. (open circles). Curve (1) is given by the calculation of Robinson (1959) from dispersion theory given by Chew et al. (1957) with $f^2 = 0{,}081$, $N^{(-)} = 0$ and $\omega_r^* = 2{,}08\,\mu$. Curve (2) corresponds to $N^{(-)} = -0{,}05$ and $f^2 = 0{,}08$.

7. Discussion of Results.

The energy dependence of positive pion photoproduction from hydrogen near threshold is conveniently represented by $/T^{+}(\theta)/^{2}$. The values obtained in this experiment for $a_o^{+} = /T^{+}(90^{o})/^{2}$ are plotted in figure 14. The solid points correspond to a selection of events for which T_{lim} = 2cm. while open circles refer to a second analysis of the results selecting only events with T_{lim} = 2,5 cm. The consistency of these two selections will be shown to justify the choice of T_{lim} = 2cm. in the selection of accepted pions.

Figure 14 also shows the theoretically predicted behaviour of a_o^{+}. Curve (1) is obtained from the calculation of Robinson (1959) using the theory given by Chew et al. (1957) with f^{2} = 0,081, $N^{(-)}$ = o and ω^{*} = 2,08μ, where $\omega^{*} + M$ is the total centre of mass energy. The lower curve (2) corresponds to a calculation with $N^{(-)}$ = -0,05 and f^{2} = 0,08. These theoretical curves have been estimated by Chew et al. to be good to 5-10% despite the approximations made in their evaluation.

Comparison of the obtained values with the theoretical curves shows that, in the energy range

E_γ = 170 to 200 Mev., while the theoretical curves rise markedly with decreasing photon energies, the experimental values obtained here are effectively constant with a value of $13,6 \pm 0,8. 10^{-30}$ cm^2/sterad.

The error markers shown in fig. 14 indicate the standard deviations for the relative errors which arise entirely from the statistical errors. An uncertainty of 5-10% in absolute beam calibration results in somewhat larger absolute errors. It is clear that the present values cannot be considered as being consistent with the theoretical predictions.

A possibility exists that this difference could arise from a lower scanning efficiency for the shorter low energy tracks. As previously mentioned rescanning of 2 000 x 4 photographs gave scanning efficiencies better than 95% for each of two separate groups of accepted pions, namely those of energies less than and greater than 25 mev. respectively.

If we supposed the scanning efficiency to vary steadily with track length throughout the analysed sample of pions, a relative difference of more than 30% in scanning efficiency for the two groups would be necessary to eliminate the discrepancy between theory and the present results. This is clearly not the case.

Alternatively, with a nearly uniform scanning efficiency for most of the accepted pions, a marked drop of scanning efficiency for the shortest tracks accepted might account for the discrepancy.

If this was the case the results obtained accepted pion with T_{lim} = 2 cm. would differ, particularly at the lowest photon energies observed, from the calculation using only pions with T_{lim} = 2,5 cm. Figure 14 shows both these treatments of the data giving essentially identical results indicating the absence of marked fall off of scanning efficiency in the range $2,0 < T < 2,5$ cm. Within the statistics the differential cross sections were identical in both cases.

Some uncertainty exists in the shape of the hardened bremsstrahlung spectrum arising from the simple assumption made, that all interacting photons are permanently removed. Departure from this behaviour would tend to favour photon intensities at lower energies at the expense of the higher energies and consequently tend to increase the discrepancy between the data and theory. In any case this effect would have a very small effect on the relative values in the energy range considered.

We must therefore conclude that since the scanning

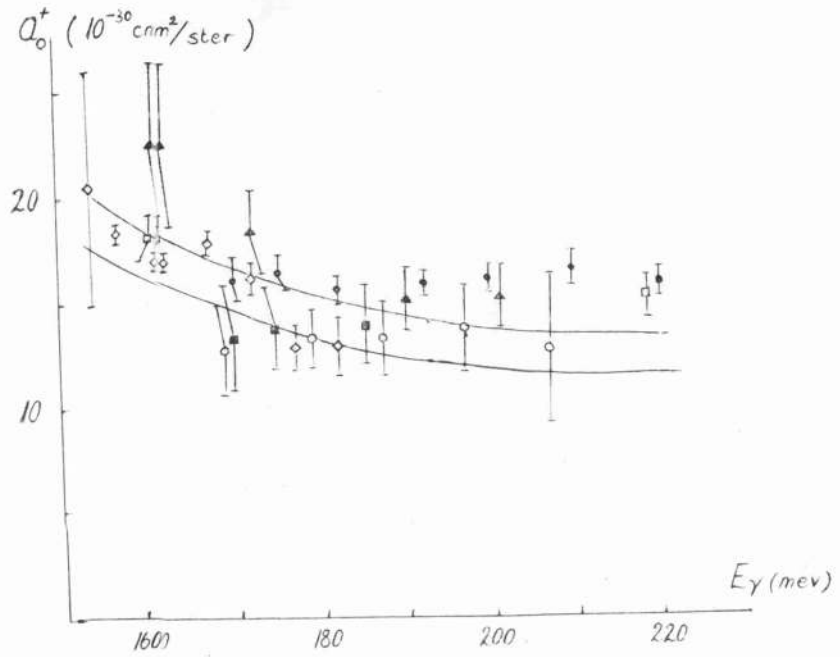

Fig.15. The present values of a_o^+ (○) are compared with the data of Beneventano et al.(1956) ● which have been increased by 10% from the original values (see text), Lewis and Azuma (1959) ■, Barbaro and Goldwasser (1959) □, Rutherglen et al.(1960) ▲ and McPherson and Kenney (1961) ◇. The upper curve is from the calculation of Robinson (1959), the lower curve corresponds to $N^{(-)} = -0,05$ and $f^2 = 0,08$.

efficiency is uniform for the pion sample analysed that the divergence between the theoretical predictions and the present results are real.

Fig.15 shows the present results compared with the early results of Beneventano et al.(1956) and also includes the results of Lewis and Azuma (1959) and Barbaro and Goldwasser (1959) and Rutherglen et al. (1960) published during the course of the present work. The recent data obtained by McPherson and Kennedy (1961) using a hydrogen bubble chamber is also included. The results of Beneventano et al. have been increased by 10% from the original values (Annual International Rochester Conf.(1960) p.26.) The results are fairly consistent and seem to indicate the value a_o^+ settling down to a constant value above 175 mev. At photon energies below 170 mev. the predicted rise of a_o^+ seems to be confirmed.

Ball (1960) using the Mandelstam representation has calculated the effect of a 2π intermediate state in photoproduction of π^+ from hydrogen. Inclusion of $\pi - \pi$ interaction appears to shift the theoretical curves as a whole and it seems unlikely that the discrepancy can be explained by a simple 2π - intermediate state.

Baldin (1960) has suggested that a comparison with the theory should be made at the centre of mass angle θ' determined by the relation

$$0,93 = k(q_o - q \cos \theta')$$

At this angle the momentum transfer equals the momentum transfer at threshold and the unphysical contribution to the dispersion integral, presumed negligible by Chew et al. (1957), is eliminated. For this case the present results give

EY (mev)	169,5	178	187
$/T^+(\ \ )/^2$ (10^{-30}cm^2/ster)	12,9 ± 2,1	13,0 ± 1,5	13,0 ± 2,8

The similarity between the results for $a_o^+ = /T^+(90^o)/^2$ and $/T^+(\theta')/^2$ shown by the present results arises from the nearly isotropic form of the angular distributions observed at these energies.

The results of Beneventano et al.(1956) as shown by Walker (1961) give a rather higher value for $/T^+(\theta')/^2$ with an energy dependence approaching that given by dispersion theory. The observed slope of the points given by Beneventano et al. (1956) arises

from the forward-backward assymetry of the angular distributions observed by Beneventano above 180 mev.

This behaviour is not borne out by the recent work of Adamovich et al. (1960 a) who obtain a more uniform angular distribution and who also consequently obtain $/T^{+}(\theta')/^{2} \approx a_{o}^{+} = 13,0.\ 10^{-30} cm^{2}/ster.$ at 185 mev. in agreement with the present results. Recently Walker and Burq (1962) have obtained an angular distribution at 185 mev substantially in agreement with Beneventano et al.

Nevertheless there appears to be a significant discrepancy between $/T^{+}(\theta')/^{2}$ given by Beneventano et al. and the dispersion theory at energies from 180 mev to 240 mev. It therefore appears that neglect of unphysical states in the dispersion relations cannot explain the failure of the theory to give a good representation of the data in the photon energy range 170 - 240 mev.

This discrepancy may arise from an insufficient evaluation of the dispersion integrals and it may be necessary to take into account contributions to the integral in addition to the important $(3/2\ ,3/2\ )$ resonance contribution. Uretsky et al.(1958) have

shown that, at least for the angular distributions, inclusion of the small P-wave amplitudes affect the theoretical predictions considerably. Further contributions to the integrals from energies above the $(3/2\ ,3/2\ )$ resonance may be important.

A further possibility is that π-π resonance effects, more complicated than the 2π intermediate state, may have considerable effect on the theory.

At energies between threshold and 170 mev the recent data of Rutherglen et al.(1960) and McPherson and Kenney(1961) indicate a rise in the value of a_o^+ near threshold (fig.15) . The latter data in particular gives agreement with the dependence predicted by dispersion theory.

Thus the dispersion theory as given by Chew et al.(1957) appears to give a fit to the data close to the threshold, but a discrepancy developes in the energy range 170 - 240 mev.

The better agreement close to threshold probably stems from the fact that near threshold the contribution of the dispersion integrals becomes small (Baldin,1960 b) and consequently the behaviour of $/T^+/^2$ is given mainly by perturbation theory and assumptions made in the evaluation of the dispersion integrals have relatively

small effect.

It therefore is indicated that although the available data indicates a threshold value of 21. 10^{-30} cm^2/ster as required to resolve the original discrepancy between low energy photoproduction and pion-scattering data, the present work indicates a deviation from the theory in the energy range EY = 170 - 211 mev. This conclusion is supported by other data for energies above 170 mev.

It therefore would be desirable to extend the measurements up to energies of 250 mev. where little data is presently available. Measurement of angular distributions in the energy range 170 - 250 Mev. would determine the energy dependence of a_o^+ and $/T(\theta')/^2$ and throw further light on the discrepancy of the 185 mev. angular distribution measurements of Adamovich et al.(1960 a) and Walker and Burq(1961).

Acknowledgements.

I wish to thank Mr. R. Irvine and the workshop staff for carrying out various modifications and additions to the bubble chamber and also Dr. W. McFarlane and the Synchtron crew for operating the Synchrotron during the experiment. Further thanks are due to Mr. R. Jennings for the use of his measuring table and to Mrs. M. Tacketts and Mrs. N. Holland for help in measuring the events and to Mrs. M. Burton for help in the preparation of the punched data cards.

I am grateful to Dr. W. Morton for his part in the analysis of the measurements, especially for writing the programme used for event reconstruction. I also wish to thank Dr. I. S. Hughes for his encouragement during the course of the work and for help in running the bubble chamber during the experiment.

Finally, I am grateful for the receipt of a University Research Studentship covering the period of this work and wish to thank Professor P. I. Dee for the use of the facilities of his laboratory.

Appendix I.

Work on $\gamma + p \rightarrow \pi^+ + n$ below $(3/2, 3/2)$ resonance.

Authors	Method	Photon Energy	Angle
Steinberger, Bishop Berkeley (1952)	Liquid H Target scintillation counters	188 - 312 (mev)	90° lab. Ang.dis.at 255me
White et al.(1952) Berkeley.	Emulsion and counters gas H target	200 - 300 mev.	45° 90° 135° lab.
Goldschmit-Clermont et al.(1953b)	$CH_2 - H$ Subtraction	320 mev.	30° 90° 150° C.M.
Jarmie et al.(1953) Berkeley	Emulsion and magnetic deflection.	278 ± 4 mev.	0°
Janes Kranshaar(1954) M.I.T.	Scintillator, Polythene-carbon subtraction	165 - 280 mev	90° lab.
Bernardini, Goldwasser Illinois (1954a)	Emulsion Liquid H target	165 - 195 mev.	40° - 159° C.M.
Jenkins et al.(1954) Cornell.	Magnetic spectrometer. Subtraction.	200,235,265 mev.	39° - 180° C.M.

Appendix I (contd).

Authors	Method	Photon Energy	Angle
Osborne et al.(1954) M.I.T.	Gas H target. Emulsions.	Meson energies 2 - 6,5 mev.	90° C.M.
Bernardini, Goldwasser Illinois (1954b)	Emulsions	167 - 230 mev.	90° C.M.
Peterson Henry (1954) Cal Tech.	Emulsion detection	167 - 233 mev.	30° - 140° lab.
Leiss et al. (1955) Illinois	Detection of positrons from π^+ absorbed in carbon round big H target	152,8 - 178,7 mev.	total.
Walker et al. (1955) Cal Tech.	Magnetic spectrometer high press H target	200 - 470 mev.	12,5° - 180° lab
Tollestrup et al.(1955) Cal Tech.	Counter telescope Gas H target	230 - 450 mev.	24° - 160° lab.
Beneventano et al. (1956) Illinois.	Emulsions Gas H Target	170 - 230 mev.	59 - 159° lab.

Appendix I (contd).

Authors	Method	Photon Energy	Angle
Richter et al.(1956) M.I.T.	Pulsed counters to reduce background at forward angles.	265 ± 13 mev.	10 - 90° C.M.
Knapp et al.(1957) Berkeley	Liquid H_2 Magnetic Deflection	260 mev.	0 - 53° C.M.
Lewis, Azuma (1959) Glasgow.	Polythene, Carbon subtraction counters.	170 - 185 mev.	90° and 115° la
Knapp et al. (1959)	Liquid H target Magnetic deflection to a counter telescope.	260, 290 mev.	0° - 160° C.M.
Gorzhevskaya et al. (1960)	CH_2 - C Subtraction Emulsions.	π energies 0,5 -6,0mev. 152,9 - 161 mev.	60° - 120°
Adamovich et al. (1960)	Emulsions.	153 - 175 mev.	90° lab.

Appendix I (contd.)

Authors	Method	Photon Energy	Angle
Adamovich et al. (1960a)	Emulsions.	185 mev.	Angular distribution
McPherson, Kenney (1961)	Hydrogen bubble chamber.	154 - 182 mev.	-
Walker, Burq (1962)	Counters. Lig H target.	185 mev.	Angular distribution.

REFERENCES

(1952a) H.L.Anderson, E.Fermi, E.A.Long, D.E.Nagle — Phys.Rev.85, 936

(1952b) H.L.Anderson, E.Fermi, D.E.Nagle, G.B.Godh — Phys.Rev.86, 793

(1952c) H.L.Anderson, E.Fermi — Phys.Rev.86, 794

(1953) H.L.Anderson, E.Fermi, R.Martin, D.E.Nagle — Phys.Rev.91, 155

(1953) C.E.Angell, J.P.Perry, — Phys.Rev.92, 835

(1955) H.L.Anderson, W.C.Davidson, U.E.Krose — Phys.Rev.100,339

(1956) Alston, Evans, Fidecaro, Newport, Von. Gierke, Williams. — Proc.Phys.Soc.69, 798

(1959) Adamovich, Kuzmicheva, Larionova, Kharlamov, — J.E.T.P. 35, 21

(1960) Adamovich, Gorzhevskaya, Larionova, Popova, Kharlamov, Yagudina, — J.E.T.P. 38, 779

(1960a) Adamovich, Kharlamor,Gorzhevskaya, Larionova, Yagudina, Popova, - see Baldin. Proc.Ann Rochester Conf.(1960) p.26.

(1951) K.A.Brueckner, R.Serber, K.M.Watson, — Phys.Rev.81, 575

(1952) K.A. Brueckner, — Phys.Rev.86, 106

(1954a) G.Bernardini, E.L.Goldwasser, — Phys.Rev.94, 729

(1954b) G. Bernardini, E.L.Goldwasser, — Phys.Rev.95, 857

(1954) D. Bodansky, A.M.Sachs, J.Steinberger — Phys.Rev.93, 1367

(1956) M. Beneventauo, G.Bernardini, D. Carlson-Lee, G. Stoppini, L. Tau, — Nuovo Cimento 4, 323.

(1958) A.M.Baldin, — Nuovo Cimento 8, 569 Nuovo Cimento, 10, 1158

(1958) M.Beneventauo G. Bernardini, G.Stoppini, L.Tau,

(1959) M.Barbaro, E.L.Goldwasser, Bull.Amer.Phys.Soc. 4. 23

(1960) J.S.Ball, Phys.Rev.Lett. 5. 73

(1960) A.M.Baldwin, Proc.Ann.Rochester.Conf.(1960) p.325

(1960b) A.M.Baldwin, J.E.T.P. 38, 416

(1960) Barnes S.W. B. Rose, G.Giacomelli, J.Ring, K.Miyake, K. Kinsey Phys.Rev.117, 226, 238.

(1952) G.F.Chew., G.C.Wick, Phys.Rev. 85, 636

(1952b) G.F.Chew, M.L.Goldberger, Phys.Rev. 87, 778

(1954) W.Chinowsky, J.Steinberger, Phys.Rev. 93, 586

(1956) G.F.Chew, F.E.Low, Phys.Rev.101, 1570, 1579.

(1956) R.Cool, O.Piccioni, D.Clark, Phys.Rev.103, 1082

(1957) J.M.Cassels, G.Fidecaro, A.M.Wetherell, J.R.Wormald, Proc.Phys.Soc. 70, 405

(1957) G.F.Chew, M.L.Goldberger, F.E.Low, Y. Nambu, Phys.Rev.106, 1337, 1345.

(1958) M.Cini, R.Gatto, E.L.Goldwasser, M.Ruderman, Nuovo Cimento 10, 242

(1959) H.Chui, E. Lomond, Ann.Phys. 6, 50

(1951) R.Durbin, L.Loar, J.Steinberger, Phys.Rev. 84, 581

(1955) Davis, J.Opt.Soc.Amer. 45. 572

(1960) Dunaĭtsev, Pantuev, Prokoshkin, Syao-wei, Khachaturyan. Proc.Ann.Rochester Conf. (1960) p.181.

(1960) M.Derrick, J.Fetkovich, T.Fields, J. Deahl, Phys.Rev.120, 1022

(1953) E.Fermi, M.Glicksman, R.Martin, D.E.Nagle, Phys.Rev.92, 161

(1958) J.Fischer, R.March, L.Marshall, Phys.Rev.109,533

(1959) G.E.Fischer, E.W.Jenkins, Phys.Rev.116,749

(1953a) Y.Clermont Goldschmidt, L.S.Osborne, M.Scott, Phys.Rev. 89, 329

(1953b) Y.Clermont Goldschmidt, L.S.Osborne, A.W.Winston Phys.Rev. 91, 468

(1954) M.Mann Gell, K.M.Watson, Rev.Nucl.Sci.4, 219

(1955) M.L.Goldberger, H.Miyazawa, R. Oehme, Phys.Rev. 99, 986

(1960) E.G.Gorzhevskaya, V.M.Popova, F.R.Yagudina, J.E.T.P. 38, 200

(1958) W.R.Hogg, E.H.Bellamy. Proc.Phys.Soc.72, 895

(1960) J.Hamilton, W.S.Woolcock, Phys.Rev.118, 291

(1953) N.Jarmie, G.V.Repp, R.S.White, Phys.Rev.91, 1023

(1954) G.S.Janes, W.L.Kraushaar, Phys.Rev.93, 900

(1954) T.L.Jenkins, D.Luckey, T.R.Palfrey, R.R.Wilson, Phys.Rev. 95, 179

(1961) D.P.Jones, P.G.Murphy, P.L.O'Neill, J.R.Wormald, Proc. Phys. Soc.77, 77

(1955) R.Karplus, M.A.Ruderman, Phys.Rev.98, 771.

(1957) E.Knapp, W.Imhof, R.W.Kenney, V.Mendez Perez. Phys Rev.107. 323

(1959) E.Knapp, R.W.Kenney, V.Mendez Perez, Phys.Rev.114, 605

(1959) E.L.Koller, A.M.Sachs, Phys.Rev.116, 760

(1959) J.A.Kuenher, A.W.Merrison, S.Tornabene, Proc. Phys.Soc. 73, 845

(1960) W.J.Kernan, C.M.York, E.L.Garwin, Phys.Rev.119, 1096

(1955) J.E.Leiss, S.Penner, C.S.Robinson. Phys.Rev. 98, 201
(1956) Ledermann et al - see C.E.R.N.Symp.1956. foot-note p.263
(1957) L.M.Lederman, K.C.Rogers, Phys.Rev.105, 247
(1959) A.J.Lazarus, W.K.H.Panofsky, F.R.Tangherlini, Phys.Rev.113, 1330
(1959) J.E.Leiss, S.Penner, Bull.Amer.Phys.Soc. 4. 273
(1959) G.M.Lewis, R.E.Azuma, Proc.Phys.Soc. 73, 873
(1959) M.J.Longo, J.A.Helland, W.N.Hess, B.J.Moyer, V.Mendez Perez. Phys.Rev.Lett.3, 568
(1959) P.D.Luckey, L.S.Osborne, J.J.Russell.Phys.Rev.Lett.3, 240

(1949) E.M.McMillan, J.M.Peterson, White Science 110, 579
(1951) R.E.Marshak Phys.Rev.82, 313
(1952) R.E.Marshak "Meson Physics" (1952)
(1955) F.E.Mills, L.J.Koestler, Phys.Rev. 98, 210
(1956) M.J.Moravcsik, Phys.Rev.104, 1451
(1957) W.S.McDonald, V.Z.Peterson, D.R.Corson, Phys.Rev.107, 577
(1958) J.H.Malmberg, C.S.Robinson, Phys.Rev.109, 158
(1958) S.Mandelstam, Phy.Rev. 112, 1344
(also P.R.115 1741, 1752)
(1961) D.McPherson, R. Kenney, Bull.Amer.Phys.Soc. 6, 523

(1956) H.P.Noyes Phys.Rev.101. 320

(1954) L.S.Osborne, V.Clermont Goldsshmidt, Phys.Rev. 95, 637
(1955) D.C.Oakley, R.L.Walker, Phys.Rev. 97, 1279
(1956) J.Orear Nuovo Cimento 4, 856

(1951) W.K.H.Panofsky, R.L.Aamodt, H.Hadley, Phys.Rev. 81, 565

(1952) W.K.H.Panofsky, J.Steinberger, J.S.Stellar, Phys.Rev. 86, 180

(1954) V.Peterson, I.G.Henry, Phys.Rev. 96, 850

(1957) G.Puppi, A.Stanghellini, Nuovo Cimento 5,1305

(1958) I. Ia. Pomeranchuk, J.E.T.P. 34, 499

(1959) C.S.Robinson, "Tables of Cross Sections for +- photoproduction from Hydrogen"

(1960) J.G.Rutherglen, J.K.Walker, D.Miller, J.M.Paterson.
Proc. Ann. Rochester Conf. 1960. page 23.

(1951) L.I.Schiff, Phys.Rev. 83, 252

(1952) A.Silverman, M.Stearns, Phys.Rev. 88, 1225

(1952) J.Steinberger, A.S.Bishop, Phys.Rev. 86, 171

(1954) M.Sands, J.G.Teasdale, R.L.Walker, Phys. Rev. 95, 592, 96, 860.

(1954) F.T.Solmitz, Phys. Rev. 94, 1779

(1954) W.J.Spry, Phys. Rev. 95, 1295

(1954) D.H.Stork, Phys. Rev. 93, 868

(1955) L.I.Schiff, "Quantum Mechanics" p. 206.

(1960) N.p. Samois Phys.Rev.Lett.4. 470

(1960) T.D.Spearman, Nuovo Cimento 15, 147

(1960) Swanson Thesis

(1954) J.Tinlot, A.Roberts, Phys.Rev. 95, 137

(1955) A.V.Tollestrup, J.C.Keck, R.M.Worlock, Phys.Rev, 99, 220

(1958) J.L.Uretsky, R.W.Kenney, E.A.Knapp, V.Mendez Perez, Phys.Rev.Lett.1. 12

(1952) L. Hove Van Phys.Rev. 88, 1358

(1950) A. Wightman Phys.Rev. 77, 521

(1951) M.N.Whitehead, C.Richman, Phys.Rev. 83, 855

(1952) R.S.White, M.J.Jacobsen, A.G. Schultz, Phys.Rev. 88, 836

(1954) K.M.Watson, Phys.Rev. 95, 228

(1955) R.L.Walker, D.C.Oakley, A.V.Tollestrup, Phys.Rev. 97, 1279

(1955) R.L.Walker, J.G.Teasdale, V.Z.Peterson, J.I.Vette, Phys.Rev. 99, 210

(1955) G.C.Wick, Rev.Mod.Phys.27, 339

(1956) K.M.Watson, J.C.Keck, A.V.Tollestrup, R.L. Walker, Phys.Rev. 101, 1159

(1957) R.R.Wilson, Nucl.Inst.1. 101

(1961) J.K.Walker, Nuovo Cimento 21, 577

(1950) C.N.Yang Phys.Rev. 77. 242

Summary of Thesis.

A Bubble Chamber Study of Pion Photoproduction from Hydrogen.

J.M.Scarr.

A review of experimental and theoretical aspects of pion photoproduction from nucleons is given together with a discussion of the relation between the photoproduction of positive pions from protons and pion-nucleon scattering. The existing experimental data is shown to be insufficient to confirm the theoretical predictions for photoproduction from hydrogen near threshold which are necessary to resolve an apparent inconsistency in the low energy data on pion-nucleon scattering and photoproduction.

A bubble chamber specially adapted for use with a high energy photon beam has been developed. The containment of any desired target material in a tube passing through the chamber and the ability to operate with either propane or freon (CF_3Br) gives a versatile method for the study of reactions induced by high energy photons. The apparatus and the choice of operating conditions are described. The method of measurement of events and their analysis from stereo-photographs is also described and the accuracy of

the analysis is discussed.

The chamber, operating as a propane chamber, has been used to study positive pion production from hydrogen for photon energies 165 - 211 Mev. Protons from neutral pion production were also recorded. The determination of the scanning efficiency for finding events and its dependanc on track length is discussed and the scanning efficiency for accepted events is shown to be high. Angular distributio for π^+-photoproduction are given and the energy dependance of the cross sections is determined. The present results lead to an essentially constant value for the usual parameter $a_o^+ = 13,3 \pm 0,8 \ .10^{-30}$ cm^2/ ster. in the energy range $E_\gamma = 169 - 206$ Mev in contrast to the marked decrease of a_o^+ with increasing photon energy predicted by dispersion theory. The results are compared with the data of other workers.

A discrepancy between theory and experimental results appears well established above 170 Mev. Possible reasons for this discrepancy are discussed and reasons are given why the theory might be expected to be more reliable closer to the photoproduction threshold.